Molecular Therapy
Original Article

cAMP/EPAC Signaling Enables ETV2 to Induce Endothelial Cells with High Angiogenesis Potential

Jae-Jun Kim,[1,2,5,6] Da-Hyun Kim,[1,2,5] Jin Young Lee,[1,2] Byung-Chul Lee,[1,2] Insung Kang,[1,2] Myung Geun Kook,[1,2] Dasom Kong,[1,2] Soon Won Choi,[1,2] Heung-Myong Woo,[3] Dong-Ik Kim,[4] and Kyung-Sun Kang[1,2]

[1]Adult Stem Cell Research Center, College of Veterinary Medicine, Seoul National University, Seoul, Republic of Korea; [2]The Research Institute for Veterinary Science, College of Veterinary Medicine, Seoul National University, Seoul, Republic of Korea; [3]College of Veterinary Medicine & Institute of Veterinary Science, Kangwon National University, Chuncheon, Gangwon, Republic of Korea; [4]Division of Vascular Surgery, Samsung Medical Center, Sungkyunkwan University School of Medicine, Seoul, Republic of Korea

Although the generation of ETV2-induced endothelial cells (iECs) from human fibroblasts serves as a novel therapeutic strategy in regenerative medicine, the process is inefficient, resulting in incomplete iEC angiogenesis. Therefore, we employed chromatin immunoprecipitation (ChIP) sequencing and identified molecular mechanisms underlying ETV2-mediated endothelial transdifferentiation to efficiently produce iECs retaining appropriate functionality in long-term culture. We revealed that the majority of ETV2 targets in human fibroblasts are related to vasculature development and signaling transduction pathways, including Rap1 signaling. From a screening of signaling pathway modulators, we confirmed that forskolin facilitated efficient and rapid iEC reprogramming via activation of the cyclic AMP (cAMP)/exchange proteins directly activated by cAMP (EPAC)/RAP1 axis. The iECs obtained via cAMP signaling activation showed superior angiogenesis *in vivo* as well as *in vitro*. Moreover, these cells could form aligned endothelium along the vascular lumen *ex vivo* when seeded into decellularized liver scaffold. Overall, our study provided evidence that the cAMP/EPAC/RAP1 axis is required for the efficient generation of iECs with angiogenesis potential.

INTRODUCTION

The therapeutic use of endothelial cells (ECs) is an attractive strategy to treat patients with traumatic and ischemic vascular diseases. In spite of the variability of clinical outcomes after autologous cell transplantation, some studies have demonstrated the clinical efficacy and safety of autologous CD34-positive cells in improving the symptoms of patients with cardiovascular diseases, such as limb ischemia,[1] angina,[2] and dilated cardiomyopathy.[3] Thus, many attempts have been made to attain patient-specific ECs from induced pluripotent stem cells (iPSCs). However, the directed endothelial differentiation of iPSCs has been challenging due to its inefficiency and poor stability of differentiated ECs in long-term culture.[4,5]

Direct reprogramming technology, which transduces lineage transcription factors into terminally differentiated cells, has emerged as an alternative strategy for the production of patient-specific ECs.[6–8] It has been reported that introducing a combination of ETS transcription factors, i.e., ETV2, FLI1, and ERG, directly transdifferentiates human amniotic cells into functional induced ECs (iECs).[8] Subsequent work by the same group revealed that the reprogramming efficiency and functionality of mouse amniotic cell-derived iECs could be promoted through the addition of protein kinase Akt1 or the transcription factor Sox17.[9] However, other researchers recently reported that ETV2 alone could directly convert human fibroblasts into functional iECs, albeit slowly and inefficiently.[6,7] To address such limitations, ETV2-mediated endothelial conversion may require enhancements in efficiency and further elucidation of underlying molecular mechanisms.

ETV2, one of the ETS family transcription factors, is a critical regulator of hematopoietic and EC development.[10,11] ETV2 deficiency even leads to embryonic lethality of animals due to the defects in blood vessel development.[10] Moreover, ETV2 could directly activate other ETS family genes, consequently establishing the ETS hierarchy.[11] Distinct from other ETS factors, ETV2 is only transiently expressed in the early phase of development.[10]

Cyclic AMP (cAMP), a second messenger generated from ATP by adenylyl cyclases, regulates a plethora of biological processes.[12] The accumulation of cAMP leads to CREB phosphorylation by cAMP-dependent protein kinase A (PKA), resulting in the activation of cAMP-responsive genes. The cAMP/PKA pathway is known to play a key role in the endothelial differentiation of mouse embryonic

Received 25 June 2019; accepted 21 November 2019;
https://doi.org/10.1016/j.ymthe.2019.11.019.

[5]These authors contributed equally to this work.

[6]Present address: Eli and Edythe Broad Center of Regeneration Medicine and Stem Cell Research, University of California San Francisco, San Francisco, CA 94143, USA.

Correspondence: Kyung-Sun Kang, Adult Stem Cell Research Center, College of Veterinary Medicine, Seoul National University, Seoul, Republic of Korea.
E-mail: kangpub@snu.ac.kr

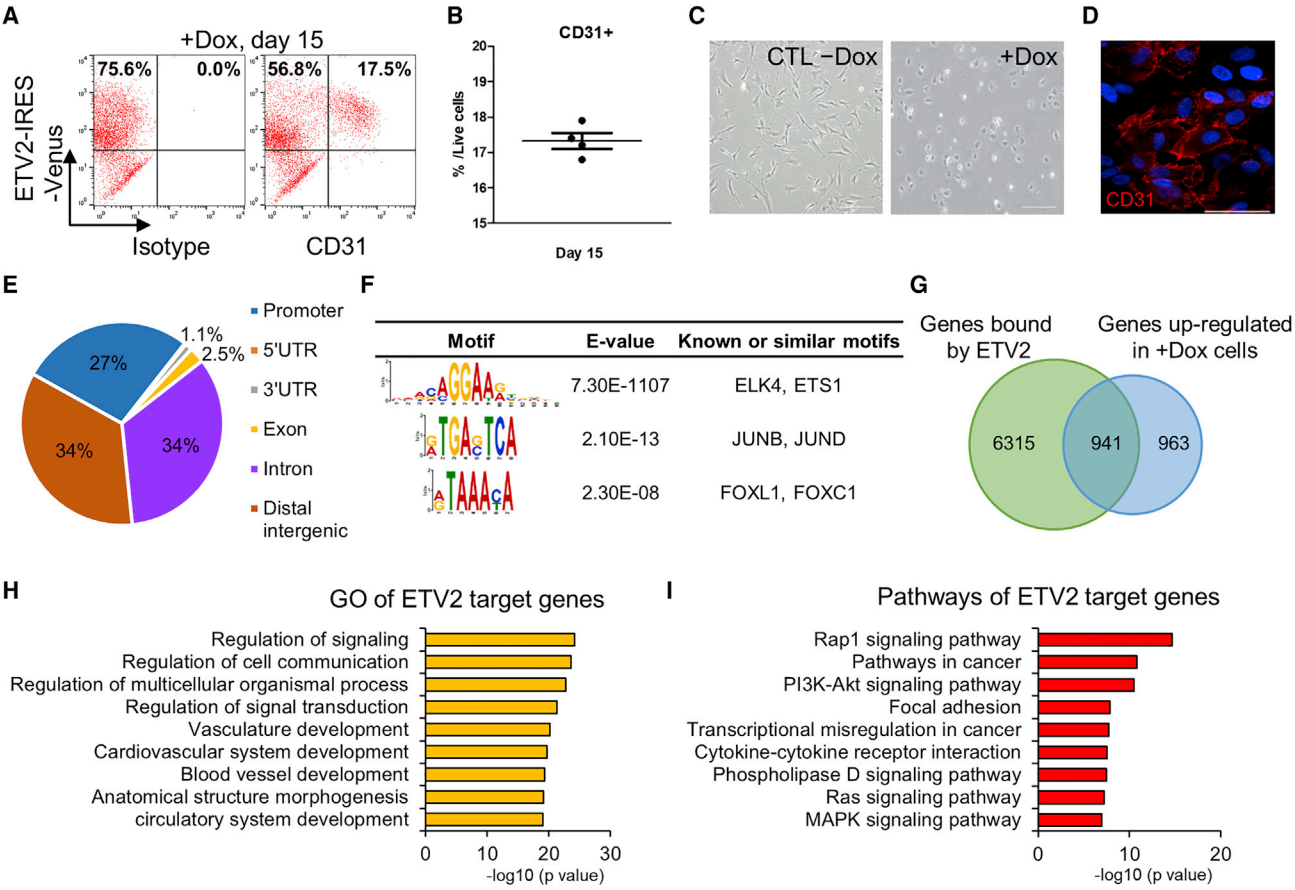

Figure 1. Characterization of ETV2's Role during Reprogramming from hDFs to iECs

(A and B) FACS analysis results (A) showing ETV2-IRES-Venus$^+$/CD31$^+$-induced ECs at day 15 with dox treatment and quantification (B) of the reprogramming efficiency. (C) Phase-contrast images of ETV2-hDFs without dox (left) and sorted CD31$^+$ iECs (right) on day 15. CTL −Dox, control cells without dox. Scale bars, 200 μm. (D) Immunocytochemical image of CD31$^+$ iECs sorted from ETV2-hDFs on day 15. Cells were immunostained for CD31 (red) and DAPI (blue). Scale bar, 50 μm. (E) ETV2 peaks genomic classification from ChIP-seq in +Dox cells. (F) Motif analysis of the ETV2 peaks. The peaks are ordered by significance. (G) Venn diagram representing the overlap of genes bound in their regulatory region (−5 kb to +1 kb plus extension up to 1 Mb distal analyzed by GREAT) and upregulated (≥2-fold) by ETV2 overexpression. (H) Gene ontology terms enriched in ETV2 target genes during reprogramming. (I) KEGG pathway analysis of ETV2 target genes.

stem cells (mESCs) through increased expression of VEGFR2 and NRP1[13] or the direct upregulation of Etv2.[14] Furthermore, another cAMP effector protein, exchange proteins directly activated by cAMP (EPAC), functions as a guanine-nucleotide-exchange factor (GEF) for small G protein Rap and acts in a PKA-independent manner.[15] However, the potential influence of cAMP signaling and its downstream effectors on iEC reprogramming from human fibroblasts has yet to be explored.

In the present study, to elucidate the mechanisms by which ETV2 drives endothelial reprogramming, we employed genome-wide analyses to define downstream targets of ETV2 in human dermal fibroblasts (hDFs). We also reported the first small molecule screen aimed at dissecting the intracellular signaling pathways that play roles in ETV2-mediated direct reprogramming. We demonstrated that forskolin, a cAMP signaling activator, enables highly efficient and rapid iEC reprogramming. Moreover, we utilized *in vitro* and *in vivo* endothelial assays to show how cAMP signaling activation can be applied to obtain stable and functional iECs.

RESULTS

Ectopic Expression of ETV2 Induces Endothelial Development Program from hDFs

The transduction of ETV2 into hDFs enables direct conversion to iECs.[6,7] To optimize this process, we infected hDFs with doxycycline (dox)-inducible lentivirus containing hemagglutinin (HA)-ETV2-internal ribosome entry site (IRES)-Venus (ETV2-hDFs).[7] We checked that ETV2-hDFs expressed ETV2 only when treated with dox (Figure S1A). Then, we observed that the population of CD31-positive cells was about 17.5% (range, 16.8%–17.9%) among the live cells on day 15 of continuous dox administration (Figures 1A and 1B). ETV2-hDFs did not express EC-specific surface markers in the absence of dox (Figure S1B). Subsequently, we obtained a pure population of CD31-positive cells by magnetic-activated cell sorting

(MACS) and characterized these cells as iECs by evaluating cobblestone morphology (Figure 1C) and anti-CD31 immunostaining (Figure 1D).

To investigate the role of ETV2 in reprogramming, we sought to identify the downstream targets of ETV2 by chromatin immunoprecipitation (ChIP) followed by DNA sequencing (ChIP-seq). HA-tagged ETV2 was immunoprecipitated from ETV2-hDFs after 7 days of dox administration. We identified 8,565 ETV2-occupied regions that corresponded mostly to the intronic (34%) and intergenic (34%) regions followed by the promoter (27%) region (Figure 1E). *De novo* motif discovery identified a highly enriched binding motif (GGAA/T) similar to a previously proposed motif in mESCs[11] (Figure 1F). Additionally, we found significant enrichment of the AP-1 motif ($E = 2.1 \times 10^{-13}$) and FOX motif ($E = 2.3 \times 10^{-8}$) in ETV2-bound regions. Next, we identified potential target genes of ETV2 by associating the ChIP peaks with nearby genes using GREAT[16] (Figure 1G). By comparing the gene-expression profiles of dox-treated cells with ChIP-seq data, 941 genes (49.4%) were found to be associated with ETV2 binding sites among the 1,904 differentially upregulated genes. Then, we functionally annotated ETV2-activated target genes and found that many of the enriched gene ontology (GO) terms were associated with vasculature development and signaling transduction (Figure 1H). KEGG pathway analyses demonstrated that ETV2 target genes were associated with Rap1, phosphatidylinositol 3-kinase (PI3K)-Akt, Ras, and mitogen-activated protein kinase (MAPK) signaling pathways, which are known to be required for normal vasculature development and angiogenesis[17,18] (Figure 1I; Table S1).

As Etv2 and its downstream targets regulate hemato-endothelial commitment of mESCs,[11] we next investigated whether key genes involved in endothelial differentiation were also bound and activated by ETV2 in hDFs. Consistent with our ChIP-seq data, we observed that ETV2 bound to regulatory elements of transcription factor-encoding genes (*SOX7*, *SOX18*, *ERG*, *FLI1*, *LMO2*, and *TAL1*) and vascular endothelial growth factor (VEGF) signaling-associated genes (*VEGFR2* and *FLT1*) (Figure S1C). We further examined whether ETV2 could modulate the epigenetic state of these genes by analyzing the level of histone H3 lysine 27 acetylation (H3K27ac), which marks active promoters and enhancers.[19,20] By ChIP-qPCR analysis, we found that ETV2 binding was accompanied with the acquisition of the active H3K27ac marks (Figure S1D). These results suggest that ETV2 converts hDFs to endothelial fate by targeting genes and signaling pathways linked to vascular development.

cAMP Signaling Pathway Activation Promotes the Reprogramming of iECs from Human Fibroblasts

Next, we attempted to overcome the slow and inefficient process of iEC generation (Figures 1A and 1B) by modulating the signaling pathways underlying ETV2-mediated reprogramming. We screened 10 small molecules based on signaling pathways linked to ETV2 targets and endothelial differentiation for their involvement in endothelial reprogramming (Figure 1I; Table S1). We quantified reprogramming efficiency by evaluating the number of CD31 and vascular endothelial (VE)-cadherin double-positive cells within the Venus (ETV2)-positive population at day 10 (Figure 2A; Table S2). Notably, SB203580, salirasib, and LY294002 inhibited the generation of $CD31^+$/VE-$cadherin^+$ iECs compared with vehicle control (DMSO), indicating that target signaling pathways of ETV2, such as MAPK, Ras, and Akt signaling, are required for hDF-to-iEC reprogramming. Interestingly, we observed that the phosphodiesterase-4 inhibitor rolipram and the cAMP signaling activator forskolin were most efficient at increasing the iEC population (Figure 2B). Combining forskolin with other small molecules did not affect the efficiency of iEC reprogramming (Figure S2A). We then varied the concentration of forskolin in the medium and determined that continuous treatment with 5 μM forskolin was optimal (Figure S2B).

To further monitor the effects of forskolin on ETV2-mediated endothelial reprogramming, we analyzed the iEC population by flow cytometry in a time-dependent manner. Forskolin treatment increased both the proportion (Figures 2C and 2D) and absolute number (Figure 2E) of $CD31^+$/VE-$cadherin^+$ iECs approximately 3.2-fold on day 7 and 1.9-fold on day 14. Moreover, forskolin did not preferentially increase the population of ETV2-infected (Venus-positive) cells (Figures S2C–S2E). This indicated that forskolin enhanced reprogramming efficiency via mechanisms other than increasing the proliferation rate of ETV2-infected cells. Immunostaining analysis on day 10 showed that forskolin-treated cultures yielded greater numbers of CD31 and VE-cadherin-positive cells (Figure 2F). Subsequently, we examined the mRNA expression levels of EC marker genes by quantitative RT-PCR (qRT-PCR) and observed increased expression levels of *PECAM1*, *VE-cadherin*, and *VWF* in forskolin-treated cells (Figure 2G). We also confirmed that ETV2-expressing cells expressed other EC surface markers, such as VEGFR2, CD34, TIE2, CLDN5, and VWF by fluorescence-activated cell sorting (FACS) analysis (Figure S2F). In addition, to explore whether forskolin could affect the reprogramming of other cell sources, we transduced retroviral ETV2 in umbilical cord blood-derived mesenchymal stem cells (UCB-MSCs). After 7 days of culture, we observed that forskolin-treated UCB-MSCs expressed higher levels of endothelial markers than did vehicle-treated UCB-MSCs (Figures S2G–S2J). Taken together, we demonstrated that forskolin, a cAMP signaling activator, enhances the endothelial reprogramming.

cAMP/EPAC/RAP1 Signaling Regulates Endothelial Reprogramming

To confirm whether the effect of forskolin was through major downstream targets of cAMP, we applied two different cAMP analogs that activated EPAC or PKA.[21] Both 8-(4-chlorophenylthio)-2′-O-methyladenosine (8-CPT-2Me)-cAMP, which selectively activates EPAC, and 8-bromoadenosine (8-Bromo)-cAMP, which activates both PKA and EPAC, increased iEC populations after 10 days of exposure (Figure 3A). We also analyzed endothelial reprogramming efficiency in the presence of two inhibitors of cAMP signaling: ESI-09, which specifically inhibits EPAC, and KT5720, which is a specific inhibitor

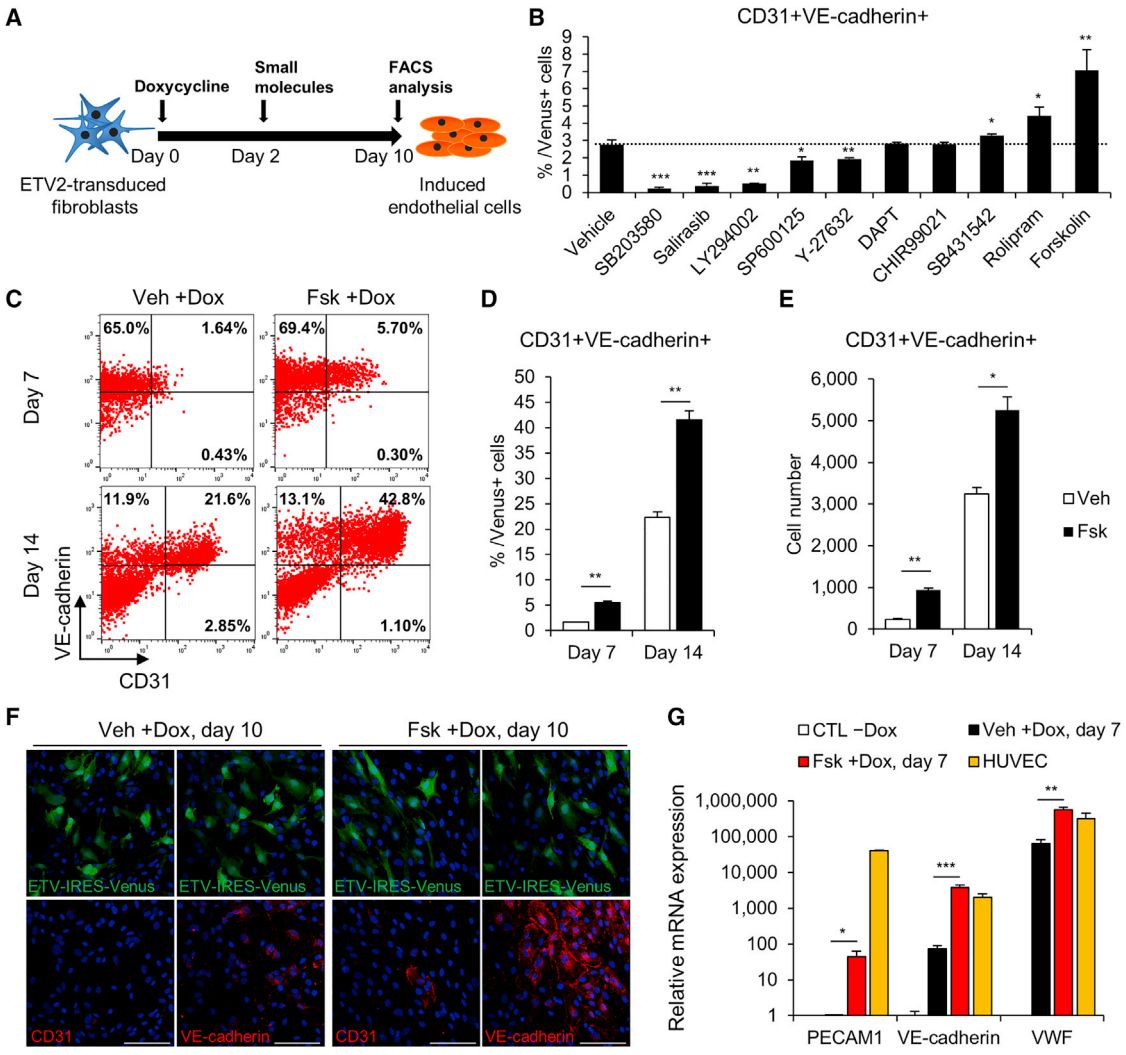

Figure 2. Small Molecule Screening Identifies the cAMP Signaling Pathway as a Facilitator of iEC Reprogramming

(A) Schematic diagram of the strategy for the screening of small molecules during iEC reprogramming. (B) Quantification of the averaged percent iECs from flow analysis at day 10 in each treatment. Gated on Venus$^+$ cells. n = 3 independent experiments; mean ± SD. *p < 0.05, **p < 0.01, ***p < 0.001 versus vehicle. (C–E) Representative FACS results (C), quantification (D), and cell numbers (E) of CD31$^+$/VE-cadherin$^+$ iECs at the indicated time points. Veh +Dox, vehicle-treated with dox; Fsk +Dox, forskolin-treated with dox. n = 3 independent experiments; mean ± SD. *p < 0.05, **p < 0.01. (F) Representative immunochemistry images for CD31 (red) and VE-cadherin (red) expression in Veh +Dox and Fsk +Dox 10 days after dox treatment. Note that the images show a heterogeneous cell population that includes either ETV2-infected (green) or uninfected cells. Scale bars, 100 μm. (G) qRT-PCR of EC-specific genes in CTL −Dox, Veh +Dox, Fsk +Dox, and HUVECs on day 7 of induction. For each group, n = 3; mean ± SD. *p < 0.05, **p < 0.01, ***p < 0.001 versus Veh +Dox.

of PKA. Both specific inhibitors reduced the iEC populations and also diminished the effects of forskolin on reprogramming (Figure 3B).

cAMP-regulated EPAC1, which is encoded by *RAPGEF3,* is known to activate small GTPase RAP1 by inducing guanosine diphosphate (GDP)/guanosine triphosphate (GTP) exchange.[15] Notably, we identified that *RAPGEF3* is directly bound and activated by ETV2, implying the involvement of cAMP/EPAC1 signaling in ETV2-mediated reprogramming (Figures 1I and 3C–3E). To investigate whether the activity of RAP1, a downstream effector of EPAC1, is regulated by ETV2, we performed pull-down assays to quantify the expression of active GTP-bound RAP1 (RAP1-GTP) protein. Interestingly, after stimulation with forskolin, the expression of RAP1-GTP was higher in ETV2-expressing cells compared with control cells (Figure 3F). Furthermore, 8-CPT-2Me-cAMP and ESI-09 regulated the amount of RAP1-GTP in ETV2-expressing cells (Figure 3G). We thus explored whether RAP1 is a key mediator of endothelial reprogramming by knocking down two isoforms of RAP1 protein, RAP1A and RAP1B (Figure 3H). After 10 days of induction, knockdown of these two genes led to a significant decrease in the generation of CD31$^+$/VE-cadherin$^+$ iECs (Figure 3I). Similar to the FACS analysis, knockdown of RAP1 caused a decrease in the mRNA levels of

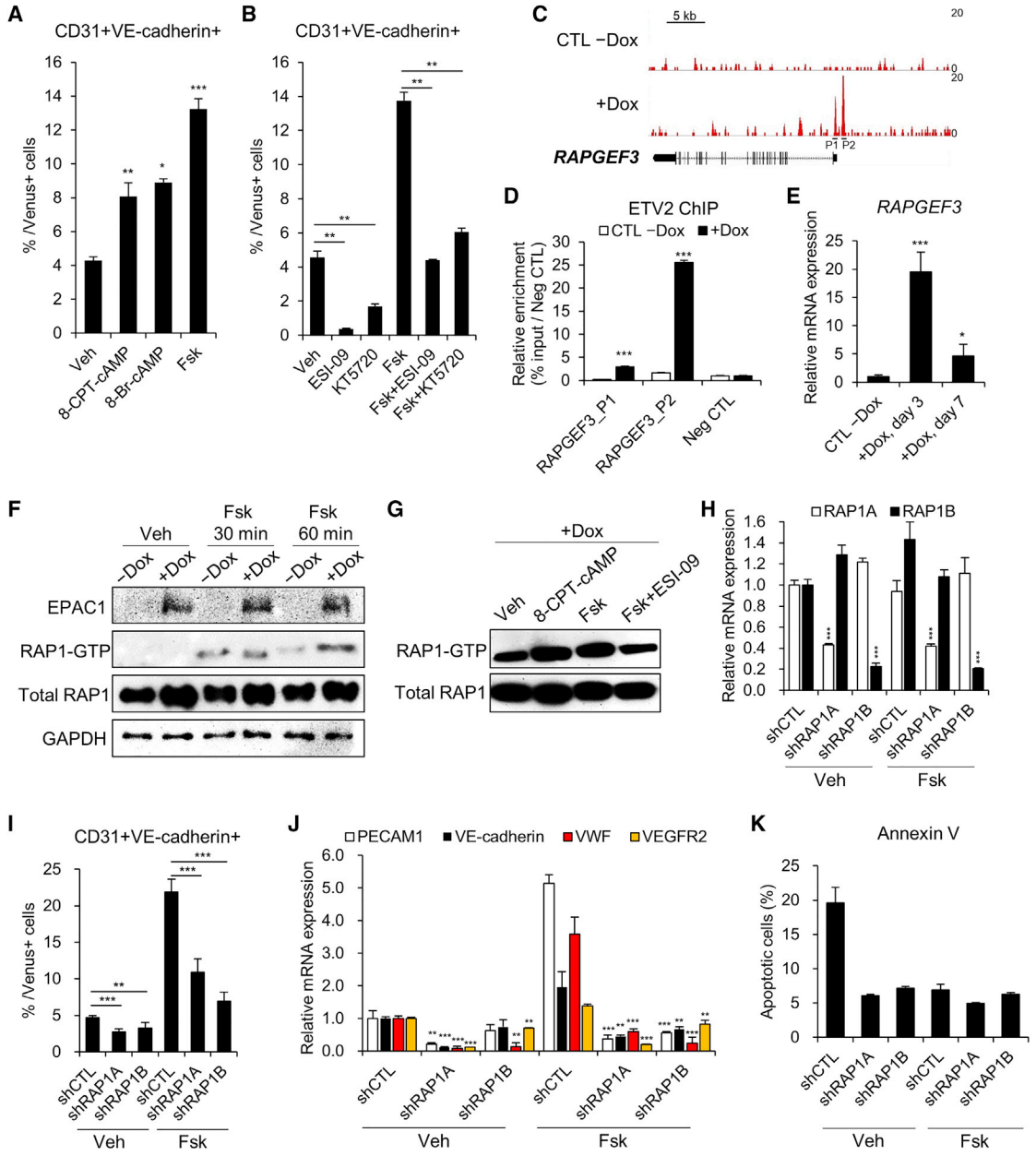

Figure 3. The cAMP/EPAC/RAP1 Axis Modulates ETV2-Mediated Reprogramming

(A) Quantification of flow cytometry analysis in iECs treated with vehicle, 100 μM 8-CPT-cAMP, 25 μM 8-Br-cAMP, or 5 μM forskolin for 10 days. After 2 days of dox treatment, the small molecules were supplemented in the medium until day 10. n = 3 independent experiments; mean ± SD. *p < 0.05, **p < 0.01, ***p < 0.001 versus vehicle. (B) Quantification of flow cytometry analysis in iECs treated with vehicle, 2.5 μM ESI-09, 3 μM KT5720, 5 μM forskolin, 5 μM forskolin + 2.5 μM ESI-09, or 5 μM forskolin + 3 μM KT5720 for 10 days. n = 3 independent experiments; mean ± SD. **p < 0.01. (C) ETV2 occupancy profile at the *RAPGEF3* locus. P1 and P2 indicate primers designed for ChIP-qPCR analysis. (D) ChIP-qPCR results showing enrichment of ETV2 at promoters of *RAPGEF3*. The regulatory region of the *POU5F1* gene was used as a negative control. For each group, n = 3; mean ± SD. ***p < 0.001 versus CTL −Dox. (E) qRT-PCR analysis of *RAPGEF3* in ETV2-hDFs without or with dox treatment on day 3 and 7 of induction. For each group, n = 3; mean ± SD. *p < 0.05, ***p < 0.001 versus CTL −Dox. (F) Western blot analysis of EPAC1, RAP1-GTP, and total RAP1 levels after the indicated treatments in −Dox and +Dox cells starved overnight. (G) Western blot analysis of RAP1-GTP and total RAP1 levels in +Dox cells treated with vehicle, 100 μM 8-CPT-cAMP, 10 μM forskolin, or 10 μM forskolin + 2.5 μM ESI-09 for 1 h. (H) qRT-PCR validation for silencing of *RAP1A* and *RAP1B* in iECs transduced with each shRNA. For each group, n = 3; mean ± SD. ***p < 0.001 versus shCTL. (I) FACS analysis of $CD31^+$/VE-$cadherin^+$ population in iECs transduced with shCTL, shRAP1A, and shRAP1B on day 10 of induction. For each group, n = 3; mean ± SD. **p < 0.01, ***p < 0.001. (J) qRT-PCR analysis of *PECAM1*, *VE-cadherin*, *VWF*, and *VEGFR2* in iECs transduced with shCTL, shRAP1A, and shRAP1B on day 7 of induction. For each group, n = 3; mean ± SD. **p < 0.01, ***p < 0.001 versus shCTL. (K) Apoptosis analysis of iECs transduced with shCTL, shRAP1A, and shRAP1B by annexin V staining on day 10 of induction. For each group, n = 3; mean ± SD.

endothelial genes, such as *PECAM1*, *VE-cadherin*, *VWF*, and *VEGFR2* at day 7 of induction (Figure 3J). Given the possibility that cells were in apoptosis during knockdown of RAP1 and thereby expressing lower endothelial markers, we confirmed that knockdown of RAP1A or RAP1B did not affect the viability of the cells by annexin V staining (Figure 3K). With these data, we found that the cAMP/EPAC/RAP1 signaling axis is an important regulatory pathway for endothelial reprogramming.

CREB Target Genes Partly Mediate iEC Reprogramming

To determine other possible mechanisms by which forskolin regulates ETV2-mediated reprogramming, we first assessed the known role of forskolin in modulating reactive oxygen species (ROS).[22,23] We observed that the exogenous expression of ETV2 during reprogramming upregulated ROS levels, whereas forskolin treatment was unable to reduce these levels (Figures S3A and S3B). We next elucidated the potential effect of forskolin on the Akt signaling pathway during endothelial reprogramming.[24] Western blot analyses of starved cells showed that forskolin, in contrast to VEGFA, could not increase phosphorylated (phospho)-AKT expression (Figure S3C).

We then proceeded to test the role of forskolin in regulating the PKA/CREB pathway during iEC reprogramming. Upon Ser133 phosphorylation by PKA, CREB translocates to the nucleus, initiating transcription of its target genes.[25] By performing co-immunoprecipitation assays, we found that phospho-CREB acts on its targets independently of a direct interaction with ETV2 (Figure S3D). Then, we tested whether forskolin increases the endogenous expression levels of ETV2 because phospho-CREB directly binds to the ETV2 promoter during hemato-endothelial differentiation from mESCs.[14] RT-PCR analysis demonstrated that endogenous ETV2 was not induced by forskolin treatment, indicating that phospho-CREB does not regulate ETV2 transcription during iEC reprogramming (Figure S3E). To further investigate the role of CREB, we selected two transcription factors (NR4A1 and JUNB), which have promoters that harbor the CRE motif, as candidate regulators of iEC reprogramming.[26,27] Forskolin treatment increased the expression of these genes by regulating the phopho-CREB binding to their promoter regions (Figures S3F–S3H). Subsequently, we transduced cells with short hairpin RNAs (shRNAs) targeting each gene to evaluate whether these genes are required in mediating iEC commitment from fibroblasts (Figure S3I). Knockdown of these two genes reduced the population of $CD31^+$/VE-$cadherin^+$ iECs and decreased the expression of endothelial-specific genes compared with control shRNA (shCTL)-infected cells (Figures S3J and S3K). Taken together, these results suggest that target genes of transcription factor CREB, in part, mediate iEC reprogramming.

cAMP Signaling Activation Induces a Vascular Genetic Program and High Angiogenesis Potential during Endothelial Reprogramming

To gain insight into the molecular-level effects of cAMP signaling activation during endothelial reprogramming, we performed RNA sequencing. In addition to human umbilical vein endothelial cells (HUVECs) and control cells not treated with dox (CTL −Dox), we compared the gene expression profiles of vehicle- and forskolin-treated ETV2-hDFs after 7 days of dox induction (Veh +Dox and Fsk +Dox). The heatmap image revealed a shift in the global gene expression patterns of ETV2-hDFs from a hDF state toward an endothelial state in 7 days of dox treatment (Figure 4A). Subsequently, we applied GO analysis to 2-fold upregulated 483 genes in forskolin-treated cells compared with vehicle-treated cells (Figure 4B). This analysis revealed that the upregulated genes in forskolin-treated cells were primarily enriched for vasculature development and angiogenesis. Furthermore, gene set enrichment analysis (GSEA) revealed a significant enrichment of vasculature development gene set in forskolin-treated cells (Figure S4A). By analyzing leading-edge genes that drive enrichment for a particular gene set, we identified forskolin-regulated leaders and associated pathways, such as angiogenesis and Notch signaling pathways (Figure S4B; Table S3). Notably, forskolin-treated cells and HUVECs showed distinct gene expression patterns compared to vehicle-treated cells in the vasculature development gene set, suggesting that forskolin enhanced endothelial reprogramming (Figure 4C; Figure S4C). To identify cell fates adopted during forskolin-mediated endothelial reprogramming, we examined the mRNA expression levels of arterial marker and venous marker genes by qRT-PCR. Interestingly, forskolin-treated cells displayed increased expression levels of arterial marker genes (*EFNB2*, *HEY1*, and *NOTCH4*) compared with vehicle-treated cells (Figures S4D and S4E). This finding suggests that forskolin-treated cells were preferentially specified to arterial fates through the activation of the Notch signaling pathway.[28]

Given that forskolin increased the expression of several genes associated with angiogenesis (Figures 4B and 4C; Table S3), we next determined whether forskolin enhances the function of iECs by using a Matrigel tubule formation assay. Because the heterogeneous nature of the reprogramming hindered the direct application of the cells in the assay, we initially sorted the cells with CD31 microbeads at day 14 of induction and observed that forskolin treatment enabled the formation of tubule structures in Matrigel (Figure S4F). However, because CD31 was barely expressed during reprogramming, we attempted to sort the reprogrammed cells with other surface markers to obtain a large number of cells. VEGFR2-positive cells have been characterized as endothelial progenitors during mesoderm specification of PSCs and have been shown to have the potential to differentiate into multiple lineages, including ECs, smooth muscle cells, and cardiomyocytes.[29] During endothelial reprogramming, we observed that the size of the VEGFR2-positive population was comparable in vehicle- and forskolin-treated ETV2-hDFs. However, the expression level of VEGR2 was higher in forskolin-treated cells from day 5 of induction (Figures 4D and 4E). Of interest, 8-CPT-2Me-cAMP promoted the expression of VEGFR2, suggesting a molecular role of the EPAC/RAP1 axis in ETV2-mediated reprogramming (Figure 4F). Thus, we sorted VEGFR2-positive cells on day 6 to remove unreprogrammed cells, and the overall purity of sorted cells was about 91% (Figures S4G and S4H). Then, the sorted cells were embedded in Matrigel to investigate angiogenesis capabilities. Even though the

amount of tubules formed in Matrigel by HUVECs was considerable, forskolin-treated VEGFR2-sorted cells showed more enhanced neoangiogenesis than did vehicle-treated VEGFR2-sorted cells (Figures 4G and 4H; Figure S4I). We additionally confirmed that forskolin-treated fibroblasts and VEGFR2-negative cells could not form the tubule structure in Matrigel, implying that the tubular networks were distinctly formed by iECs (Figures S4J and S4K). Collectively, these data demonstrated that this cAMP signaling activator plays a role in improving the reprogramming efficiency and *in vitro* angiogenesis capacity of iECs.

cAMP Signaling Activated iECs Increase Vascularity in the Ischemic Hindlimb

On the basis of *in vitro* results, we further evaluated whether cAMP signaling activation enhances angiogenic activity of iECs *in vivo*. We surgically ligated and transected the femoral artery in nude mice to establish a hindlimb ischemia model for efficient blood vessel regeneration.[30,31] Four types of cells were intramuscularly transplanted into the ischemic hindlimbs: control cells without dox (CTL −Dox), vehicle- and forskolin-treated VEGFR2-sorted cells (Veh +Dox and Fsk +Dox), and HUVECs. For 14 days post-surgery, mice implanted with forskolin-treated cells and HUVECs showed improved recovery of blood flow compared to control cell-implanted mice (Figure 5A). Notably, transplantation of forskolin-treated cells significantly enhanced blood perfusion and limb salvage in the ischemic hindlimb compared with vehicle-treated cells (Figures 5B and 5C). After isolectin B4 was intravenously administered, the gastrocnemius muscles of each group were dissected and analyzed via blood vessel quantification in the ischemic regions. The number of vessels (rhodamine-positive) was quantified from randomly selected images. The results showed greater levels of angiogenesis in the forskolin-treated cell group than those observed in the vehicle-treated cell group (Figures 5D and 5E). These findings indicate that cAMP signaling activated iECs retain superior angiogenic capacity, augmenting neovascularization *in vivo*.

Long-Term Cultured iECs Exhibit Morphological and Functional Characteristics of ECs

We next determined whether iECs show additional functional characteristics other than angiogenesis potential. VEGFR2-sorted iECs showed reduced proliferation, thereby limiting its long-term passaging and culture. Considering the ChIP-seq data, we reasoned that ETV2 may directly repress cell cycle-related genes, such as *KIF14* and *CKS2*, in hDFs (Figure S5). Thus, following a protocol used to generate late iECs,[6] we cultured and passaged VEGFR2-sorted iECs without dox and then retreated them with dox from day 14. We observed that forskolin-treated cultures yielded a larger population of $CD31^+$/VE-$cadherin^+$ cells during a 42-day period compared with vehicle-treated cultures (Figures 6A and 6B). We also checked that VEGFR2-sorted iECs expressed other endothelial markers, such as TIE2 and CD34 (Figure S6A). Interestingly, VEGFR2-sorted iECs on day 24 displayed a more homogeneous cobblestone morphology than did cells on day 7 (Figures 4G and 6C). Additionally, forskolin treatment maintained the expression of VEGFR2 (Figure S6B) and increased the angiogenesis phenotype, as shown by the Matrigel tubule formation assay (Figures 6C and 6D; Figure S6C). To characterize these cells further, we performed qRT-PCR analysis and observed that forskolin upregulated the expression of endothelial marker genes (*PECAM1*, *VE-cadherin*, *VWF*, and *VEGFR2*), arterial marker genes (*NOTCH4* and *HEY1*), and vasculature development-associated genes (*SOX18*, *FOXO1*, *TSPAN12*, and *EDN1*) in VEGFR2-sorted iECs (Figure 6E). Of interest, forskolin treatment reduced the expression of mesenchymal marker genes, such as *THY1*, *FSP1, NGFR, SNAI2, and TWIST1*, in VEGFR2-sorted iECs, implying the silence of fibroblasts gene signature (Figure 6F). Additionally, to investigate the mesenchymal identity of VEGFR2-sorted iECs, we checked the expressions of THY1 and FSP1 proteins after 35 days of culture. Although THY1-positive cells remained among the CD31-positive population, forskolin significantly reduced the number of THY1-positive cells compared to vehicle treatment (Figures S7A–S7C). We also observed that FSP1 was barely expressed in forskolin-treated cells, suggesting the suppression of mesenchymal identity by forskolin (Figure S7D). Based on these results, we cultivated the forskolin-treated VEGFR2-sorted iECs (Fsk-iECs) without dox treatment in large quantities and assessed other vascular functions of the cells.

First, we measured barrier tightness using fluorescein isothiocyanate (FITC)-dextran in Fsk-iECs and HUVECs after treatment with various inflammatory cytokines and observed increased permeability across the monolayer (Figure S6D). We confirmed the uptake of fluorescently labeled acetylated low-density lipoprotein (LDL) in Fsk-iECs and HUVECs, which is characteristic of normal ECs (Figure S6E). Moreover, to demonstrate the integration of Fsk-iECs into vascular networks *in vivo*, carboxyfluorescein diacetate succinimidyl ester (CFDA)-labeled Fsk-iECs were embedded in Matrigel and subcutaneously injected into the flanks of BALB/c nude mice. We observed that Fsk-iECs (CFDA and rhodamine double-positive) could engraft into existing host vasculature (Figure S6F). Given these results, Fsk-iECs appear to acquire functional features of vascular ECs via direct reprogramming.

Fsk-iECs Can Re-endothelialize the Acellular Rat Liver Scaffold

In our previous study, we successfully reconstructed vasculature trees within decellularized liver scaffolds using EA.hy926 ECs derived from immortalized HUVECs.[32] In an effort to prove the vasculogenesis of long-term cultured Fsk-iECs, we developed an *ex vivo* two-phase culture strategy, which facilitates the vascular modeling of decellularized rat liver scaffold. In this strategy, VEGFR2-sorted iECs, expanded without dox treatment, were seeded and cultured in the scaffold using perfusion bioreactor systems to maintain their viability. In phase 1, the cells were injected to engraft into the scaffold and expanded for 7 days without dox. In phase 2, resupplementation of dox and forskolin in the perfusion medium promoted functional maturation of the cells to form confluent endothelium along the vascular channel in another 14 days (Figure 6G).

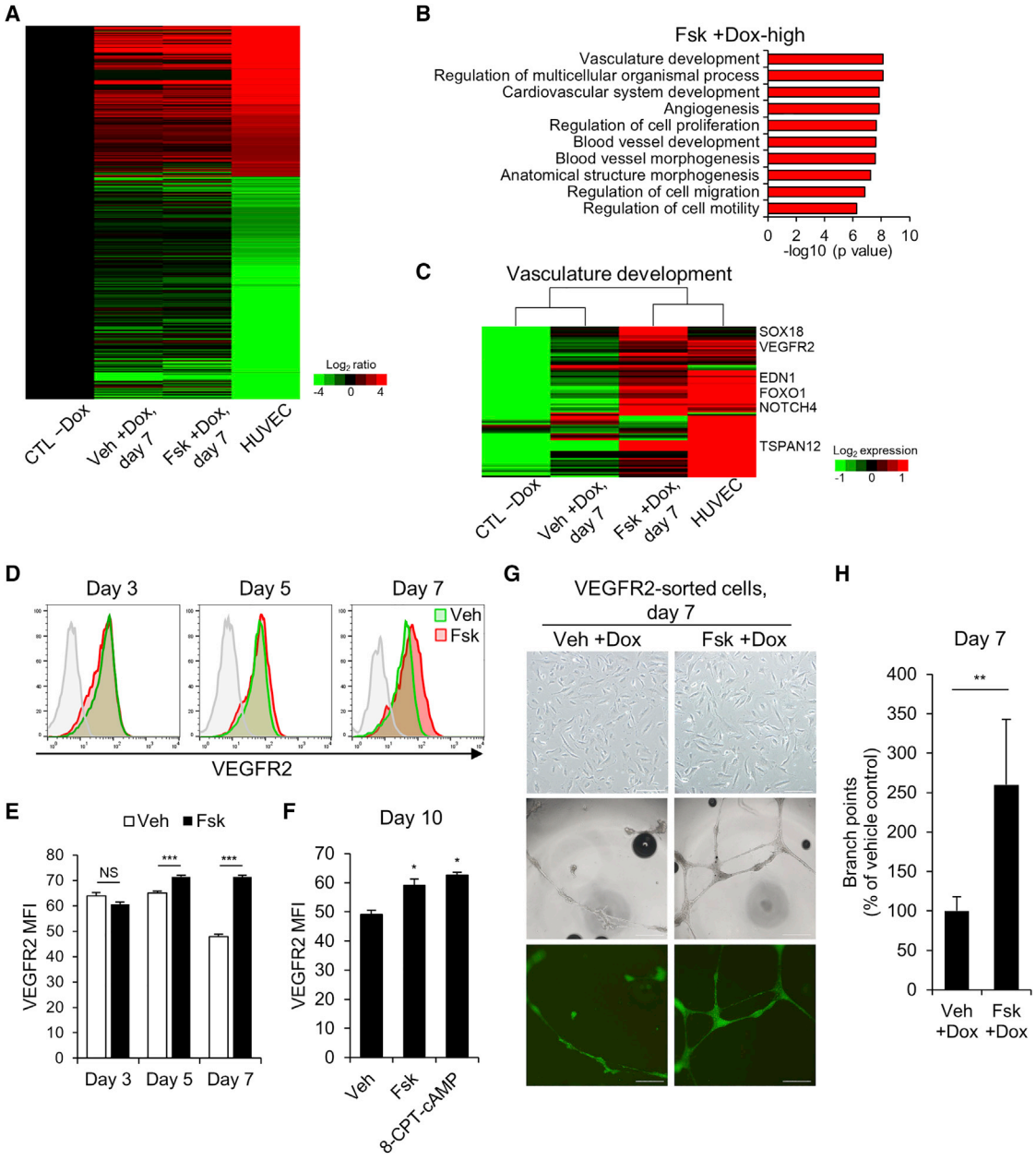

Figure 4. cAMP Signaling Activation Induces Endothelial Gene Expression and Enhances Angiogenesis Potential

(A) Heatmap representing the log-fold changes of group Veh +Dox, Fsk +Dox, and HUVECs compared to CTL −Dox. ETV2-hDFs were treated without or with dox for 7 days. Genes that were differentially expressed by more than 4-fold between CTL −Dox and HUVECs are represented. CTL −Dox, control cells without dox. (B) GO term enrichment analysis of the genes that were differentially expressed by ≥2-fold in Fsk +Dox compared with Veh +Dox. The top 10 GO terms for biological processes are shown. (C) Heatmap showing the expression of representative genes involved in vasculature development. (D and E) Representative FACS profiles (D) and quantification (E) of mean fluorescence intensity (MFI) of VEGFR2 in Veh +Dox (green) and Fsk +Dox (red) at day 3, 5, and 7 post-induction. For each group, n = 3; mean ± SD. ***$p < 0.001$. (F) MFI of VEGFR2 in iECs treated with vehicle, 100 μM 8-CPT-cAMP, or 5 μM forskolin for 10 days. For each group, n = 3; mean ± SD *$p < 0.05$. (G) Phase-contrast images (top) of VEGFR2-sorted cells from ETV2-hDFs on day 7 of induction. Scale bars, 200 μm. Representative phase-contrast images (middle) and ETV2-Venus fluorescence images (bottom) of tubular structures 24 h after plating on Matrigel. Scale bars, 500 μm. (H) Quantification of branching points formed during *in vitro* tubulogenesis. n = 4 independent experiments; mean ± SD. **$p < 0.01$.

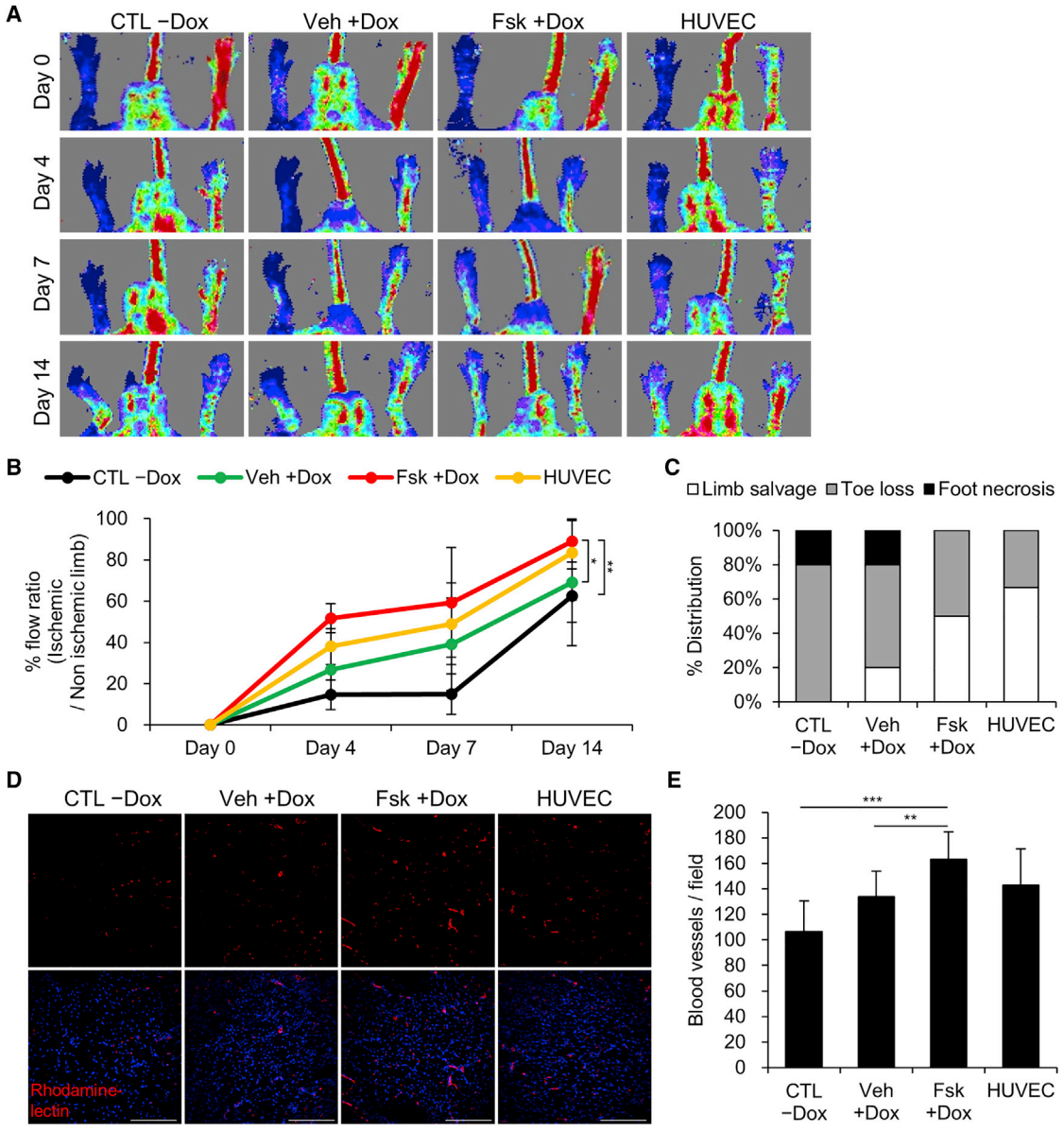

Figure 5. cAMP Signaling-Activated iECs Improve Angiogenesis in Hindlimb Ischemia

(A and B) After transplantation of CTL −Dox, Veh +Dox and Fsk +Dox (VEGFR2-sorted after 5 days of dox induction), and HUVECs, blood reperfusion of ischemic limbs was analyzed via laser Doppler imaging (LDI) by 14 days post-surgery. Representative images of LDI analysis (A) and the ratio of blood perfusion (left injured limb/right normal limb) (B) are shown. For each group, n = 5–6; mean ± SD. *$p < 0.05$, **$p < 0.01$ by two-way ANOVA. (C) At 18 days post-surgery, ischemic limbs were examined visually to determine severity of toe and foot necrosis in each group. (D and E) Representative immunofluorescence images (D) and quantification (E) of rhodamine-lectin-stained blood vessels (red) in the gastrocnemius muscle sections on day 18 post-surgery. Nuclei were counterstained with DAPI (blue). Scale bars, 100 μm. For each group, n = 12; mean ± SD. **$p < 0.05$, ***$p < 0.001$.

To measure the extent of endothelialization, we harvested the cell-seeded scaffolds after phase 1 and phase 2 culture (Figure 6H). Picrosirius red staining was carried out to evaluate cellular distribution within the scaffold for each group. After phase 1 culture, the cells engrafted into the scaffold but did not form elaborate vascular networks. After phase 2 culture, Fsk-iECs developed complete endothelialization, surrounding the vessel lumen of the scaffold (Figure 6I). To determine the proportion of reprogrammed cells contributing to endothelialization, we performed immunostaining of the tissue sections. Consistent with histological examinations, vessel-like structures comprising isolectin B4, VE-cadherin, and CLDN5-positive cells were detected after phase

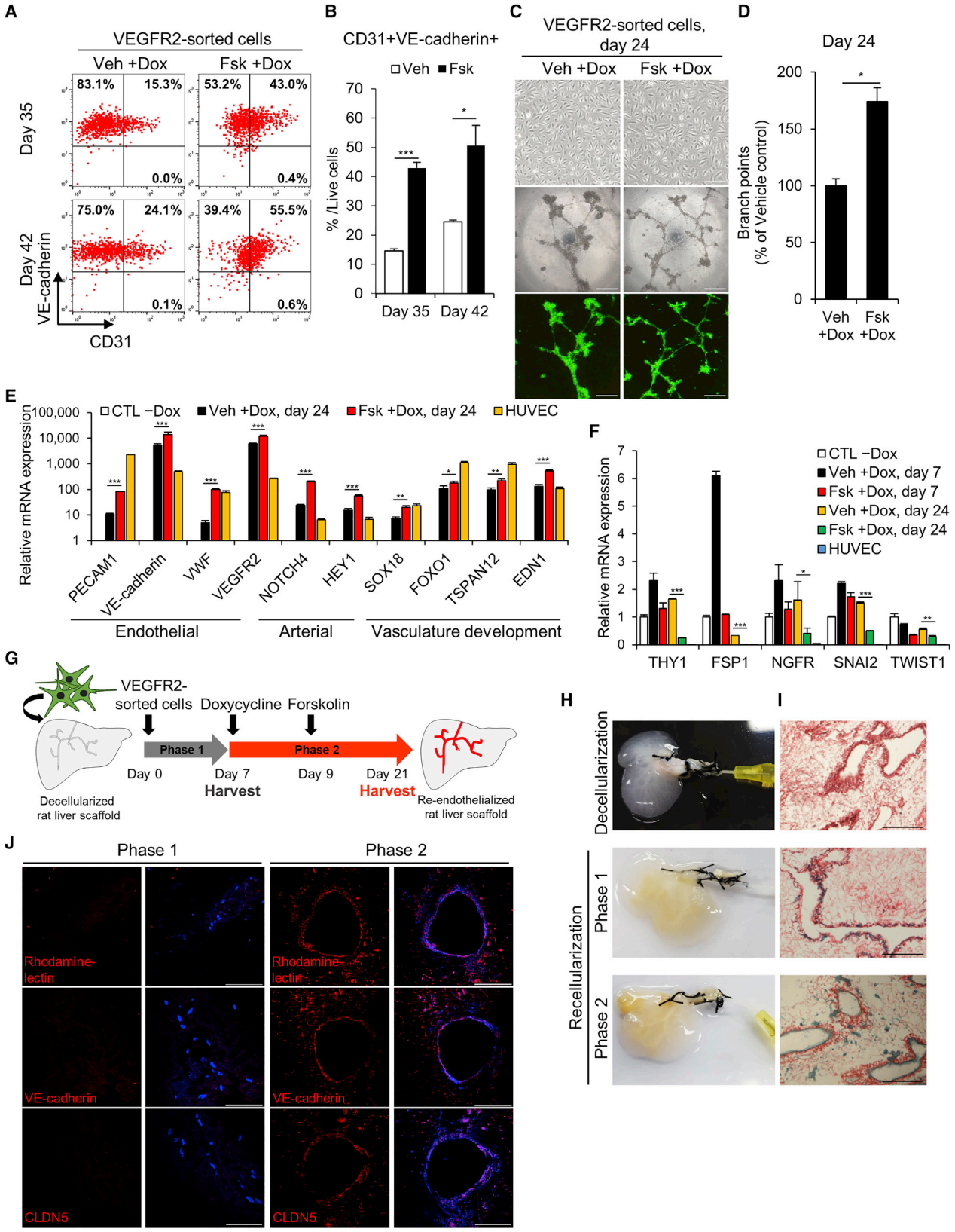

(legend on next page)

2 culture (Figure 6J). Taken together, these results support that Fsk-iECs are capable of maintaining their characters and forming aligned vascular networks in tissue-engineered constructs.

Fsk-iECs Show Protective Effects on Ischemia-Induced Severe Injury

To further assess whether long-term cultured Fsk-iECs are applicable for therapeutic uses, we intramusculary transplanted the cells after induction of severe hindlimb ischemia by simultaneous excision of the femoral artery, vein, and its branches. Mice implanted with Fsk-iECs and HUVECs exhibited limb tissues partially protected from necrosis, whereas mice implanted with CTL −Dox experienced severe ischemia resulting in massive muscle degeneration (Figures S8A–S8D). Quantification of blood vessels in gastrocnemius muscle showed greater levels of angiogenesis in the Fsk-iECs and HUVECs groups than those observed in the CTL −Dox group (Figures S8E and S8F). Moreover, we confirmed that Fsk-iECs and HUVECs could be engrafted into the newly generated vessels in ischemic himdlimbs (Figures S8G and S8H). Collectively, we corroborated that Fsk-iECs displayed angiogenic potential *in vivo* and could be incorporated to host vasculature, both of which are certainly necessary for therapeutic applications.

DISCUSSION

ETV2 is a known master regulator of hemato-endothelial development;[33] however, little is known about its molecular role in hDF-to-iEC reprogramming. In this study, by integrating genome-wide ChIP-seq and RNA sequencing (RNA-seq) analyses, we revealed target genes of ETV2, yielding insights into the mechanisms by which ETV2 drives endothelial reprogramming and the molecular links between ETV2 and signaling pathways. The indispensable roles of ETV2-regulated Notch and VEGF signaling during development have been well described.[34] However, the finding that ETV2 directly regulates EPAC1, an important regulator of Rap1 signaling, allowed us to infer its novel role in ETV2-mediated endothelial reprogramming. The cAMP/EPAC pathway elevates endothelial barrier function and regulates remodeling of ECs.[35] In the context of development, EPAC promotes hematopoietic differentiation from human PSCs by reducing ROS levels.[23] Moreover, although EPAC-deficient mice do not exhibit lethal phenotypes,[15] the knockout of Rap1 in mice leads to cardiovascular defects and impaired angiogenesis,[36] suggesting compensatory roles of other RapGEFs in maintaining Rap1 functions in EPAC-deficient mice. Therefore, considering that selective activation and blockade of EPAC altered the population of iECs, we surmise that the cAMP/EPAC/Rap1 pathway may be involved in ETV2-related pathological angiogenesis, such as tumor angiogenesis[37] and ischemic injury-mediated neo-angiogenesis.[38]

To date, considerable progress has been made to generate ECs by directed differentiation from PSCs.[39–41] Researchers have investigated various signaling pathways involved in this process and have attempted to enhance the efficiency and quality of ECs.[4,29,39] Thus, in an effort to improve the reprogramming process, we screened small molecules based on signaling pathways linked to endothelial differentiation and found that the cAMP signaling activator forskolin enabled a highly rapid and efficient generation of iECs from hDFs. However, we observed that some signaling modulators showed distinct effects on directed differentiation and ETV2-mediated reprogramming. This implies that these two processes may generate ECs via different molecular and signaling cascades. Furthermore, one report described that inhibition of transforming growth factor β (TGF-β) signaling enabled iEC reprogramming from amniotic cells by regulating VEGFR2 phosphorylation.[8] However, we observed that treatment of cells with SB431542 alone or with forskolin had minimal effects on the efficiency of generating $CD31^+$/VE-$cadherin^+$ populations. This may have resulted from different cell sources and combination of transcription factors used in each study; specifically, our study used ETV2 alone-infected human fibroblasts.

Our transcriptome analyses allowed us to elucidate the molecular effects of cAMP signaling activation in endothelial reprogramming. Treatment of forskolin seems to preferentially lead to the formation of endothelial-like cells via upregulation of vascular development-related genes. Above all, it is noteworthy that the activation of EPAC increases the expression of VEGFR2, as phosphorylated VEGFR2 upon VEGF binding triggers several signaling cascades and critically regulates vascular development and angiogenesis.[42] Considering the finding of a previous report that a constitutive active form of PKA regulated the expression of VEGFR2 in a directed differentiation of mESCs to ECs,[13] our observation supports a possible role of cAMP/EPAC signaling in the regulation of differentiation.

Furthermore, forskolin is known to enhance other types of reprogramming, such as induced neurons[22] or iPSCs,[43,44] through regulation of anti-oxidative pathways[22] or chromatin accessibility.[45] More

Figure 6. Vasculogenic Ability of Long-Term Cultured Fsk-iECs

(A and B) Representative FACS results (A) and quantification (B) of $CD31^+$/VE-$cadherin^+$ iECs that are derived from VEGFR2-sorted cells at the indicated time points. Note that dox was readministered with vehicle or forskolin from day 14. For each group, n = 3; mean ± SD. *p < 0.05, ***p < 0.001. (C) Phase-contrast images of VEGFR2-sorted cells at day 24 post-induction (top). Scale bars, 200 μm. Representative phase-contrast images (middle) and ETV2-Venus fluorescence images (bottom) of tubular structures 24 h after plating on Matrigel are shown. Scale bars, 500 μm. (D) Quantification of branch points formed during *in vitro* tubulogenesis. For each group, n = 4; mean ± SD. *p < 0.05. (E and F) qRT-PCR of endothelial, arterial and vasculature development-related genes (E) and mesenchymal marker genes (F) in CTL −Dox, HUVECs, and VEGFR2-sorted cells on day 24 of induction. For each group, n = 3; mean ± SD. *p < 0.05, **p < 0.01, ***p < 0.001. (G) Schematic diagram of the strategy used for recellularization of VEGFR2-sorted cells into rat acellular liver scaffolds. (H and I) Gross images (H) and representative picrosirius red-stained sections (I) of rat liver extracellular matrix. Decellularized liver (top); recellularized liver with VEGFR2-sorted cells after phase 1 (middle); recellularized liver harvested at the end of phase 2 (bottom). For each group, n = 2. Scale bars, 200 μm. (J) Representative confocal microscopic images of recellularized vessel structures on day 7 and day 21. The sections of each group were stained with rhodamine-lectin (top), VE-cadherin (middle), and CLDN5 (bottom). Nuclei were stained with DAPI (blue). Scale bars, 100 μm.

than that, a recent study revealed that the addition of cAMP promoted DNA demethylation by regulating the amount of 5-hydroxymethylcytosine.[46] Thus, it will be interesting to assess in future studies whether forskolin affects metabolism or chromatin architecture underlying ETV2-mediated reprogramming.

Our findings demonstrated an advanced method that could enhance the reprogramming efficiency and quality of iECs. We proposed diverse applications of these cells. Specifically, these cells could be used for the treatment of ischemic diseases and for various endothelial platforms. By applying Matrigel plug assays and a hindlimb ischemia model, Fsk-iECs were shown to be capable of integrating into host vasculature *in vivo*. However, these assays merely recapitulate angiogenesis, which is the growth of new vasculature extended from existing vessels. In this regard, we provided a newly developed platform for validating long-term endothelialization by using a decellularized liver scaffold. By extension, this approach may lay the groundwork for engineering human hepatic tissue with functional vasculature because well-vascularized networks are indispensable for liver regeneration. Thus, these characteristics of Fsk-iECs provide a special advantage for stably producing iECs for applications in regenerative medicine.

Even though there was a limitation that iECs were not readily expandable, we could overcome this issue by adopting the strategy that VEGFR2-sorted cells were maintained with dox-withdrawn medium for proliferation and then re-induced for rapid maturation. With this approach, we could secure sufficient scales without cell senescence and the loss of characteristics. To this end, with the scalability of iECs, future applications of iECs for the GMP system and therapeutics will be considerable.

MATERIALS AND METHODS

Generation of iECs

To generate iECs, human dermal fibroblasts transduced with ETV2 were seeded on collagen type I-coated (20 μg/mL, Corning) plates containing FGM-2. After expansion of the cells, the medium was changed to EGM-2 supplemented with doxycycline (Sigma) and replenished every other day. For small molecules treatment, reagents were purchased from the following sources: SB203570, Salirasib, LY294002, SP600125, CHIR99021, and SB431542 from Sigma; rolipram, forskolin, DAPT, KT5720, and ESI-09 from Cayman Chemical; and 8-Bromo-cAMP and 8-CPT-2Me-cAMP from Tocris.

SUPPLEMENTAL INFORMATION

Supplemental Information can be found online at https://doi.org/10.1016/j.ymthe.2019.11.019.

AUTHOR CONTRIBUTIONS

J.-J.K. and D.-H.K. designed and performed the study. J.-J.K., D.-H.K., J.Y.L, B.-C.L., D.K., and I.K. performed the experiments. M.G.K. helped to analyze ROS levels. S.W.C., D.-I.K., and H.-M.W. contributed discussion. K.-S.K. supervised the study and contributed to writing.

CONFLICTS OF INTEREST

The authors declare no competing interests.

ACKNOWLEDGMENTS

We thank Dr. Rimpei Morita at Keio University for the CSII-EF-HA-ETV2-IRES-Venus plasmid. We are grateful to Dr. Young-sup Yoon at Emory University School of Medicine and Dr. Kyung-Rok Yu at Catholic University of Korea for experimental advice. We also thank Dr. Byeong-Cheol Kang, Dr. Won-Woo Lee, and Dr. Jae-Hak Park at Seoul National University for helpful discussions. This work was carried out with the support of the Cooperative Research Program for Agriculture Science & Technology Development (Project No. PJ01100201), Rural Development Administration, Republic of Korea.

REFERENCES

1. Losordo, D.W., Kibbe, M.R., Mendelsohn, F., Marston, W., Driver, V.R., Sharafuddin, M., Teodorescu, V., Wiechmann, B.N., Thompson, C., Kraiss, L., et al.; Autologous CD34+ Cell Therapy for Critical Limb Ischemia Investigators (2012). A randomized, controlled pilot study of autologous CD34$^+$ cell therapy for critical limb ischemia. Circ. Cardiovasc. Interv. *5*, 821–830.

2. Velagapudi, P., Turagam, M., Kolte, D., Khera, S., Hyder, O., Gordon, P., Aronow, H.D., Leopold, J., and Abbott, J.D. (2019). Intramyocardial autologous CD34+ cell therapy for refractory angina: a meta-analysis of randomized controlled trials. Cardiovasc. Revasc. Med *20*, 215–219.

3. Vrtovec, B., Poglajen, G., Lezaic, L., Sever, M., Domanovic, D., Cernelc, P., Socan, A., Schrepfer, S., Torre-Amione, G., Haddad, F., and Wu, J.C. (2013). Effects of intracoronary CD34$^+$ stem cell transplantation in nonischemic dilated cardiomyopathy patients: 5-year follow-up. Circ. Res. *112*, 165–173.

4. Israely, E., Ginsberg, M., Nolan, D., Ding, B.S., James, D., Elemento, O., Rafii, S., and Rabbany, S.Y. (2014). Akt suppression of TGFβ signaling contributes to the maintenance of vascular identity in embryonic stem cell-derived endothelial cells. Stem Cells *32*, 177–190.

5. James, D., Nam, H.S., Seandel, M., Nolan, D., Janovitz, T., Tomishima, M., Studer, L., Lee, G., Lyden, D., Benezra, R., et al. (2010). Expansion and maintenance of human embryonic stem cell-derived endothelial cells by TGFβ inhibition is Id1 dependent. Nat. Biotechnol. *28*, 161–166.

6. Lee, S., Park, C., Han, J.W., Kim, J.Y., Cho, K., Kim, E.J., Kim, S., Lee, S.J., Oh, S.Y., Tanaka, Y., et al. (2017). Direct reprogramming of human dermal fibroblasts into endothelial cells using ER71/ETV2. Circ. Res. *120*, 848–861.

7. Morita, R., Suzuki, M., Kasahara, H., Shimizu, N., Shichita, T., Sekiya, T., Kimura, A., Sasaki, K., Yasukawa, H., and Yoshimura, A. (2015). ETS transcription factor ETV2 directly converts human fibroblasts into functional endothelial cells. Proc. Natl. Acad. Sci. USA *112*, 160–165.

8. Ginsberg, M., James, D., Ding, B.S., Nolan, D., Geng, F., Butler, J.M., Schachterle, W., Pulijaal, V.R., Mathew, S., Chasen, S.T., et al. (2012). Efficient direct reprogramming of mature amniotic cells into endothelial cells by ETS factors and TGFβ suppression. Cell *151*, 559–575.

9. Schachterle, W., Badwe, C.R., Palikuqi, B., Kunar, B., Ginsberg, M., Lis, R., Yokoyama, M., Elemento, O., Scandura, J.M., and Rafii, S. (2017). Sox17 drives functional engraftment of endothelium converted from non-vascular cells. Nat. Commun. *8*, 13963.

10. Lee, D., Park, C., Lee, H., Lugus, J.J., Kim, S.H., Arentson, E., Chung, Y.S., Gomez, G., Kyba, M., Lin, S., et al. (2008). ER71 acts downstream of BMP, Notch, and Wnt signaling in blood and vessel progenitor specification. Cell Stem Cell *2*, 497–507.

11. Liu, F., Li, D., Yu, Y.Y., Kang, I., Cha, M.J., Kim, J.Y., Park, C., Watson, D.K., Wang, T., and Choi, K. (2015). Induction of hematopoietic and endothelial cell program orchestrated by ETS transcription factor ER71/ETV2. EMBO Rep. *16*, 654–669.

12. Corrigan, R.M., and Gründling, A. (2013). Cyclic di-AMP: another second messenger enters the fray. Nat. Rev. Microbiol. *11*, 513–524.

13. Yamamizu, K., Kawasaki, K., Katayama, S., Watabe, T., and Yamashita, J.K. (2009). Enhancement of vascular progenitor potential by protein kinase A through dual induction of Flk-1 and Neuropilin-1. Blood *114*, 3707–3716.

14. Yamamizu, K., Matsunaga, T., Katayama, S., Kataoka, H., Takayama, N., Eto, K., Nishikawa, S., and Yamashita, J.K. (2012). PKA/CREB signaling triggers initiation of endothelial and hematopoietic cell differentiation via Etv2 induction. Stem Cells *30*, 687–696.

15. Lezoualc'h, F., Fazal, L., Laudette, M., and Conte, C. (2016). Cyclic AMP sensor EPAC proteins and their role in cardiovascular function and disease. Circ. Res. *118*, 881–897.

16. McLean, C.Y., Bristor, D., Hiller, M., Clarke, S.L., Schaar, B.T., Lowe, C.B., Wenger, A.M., and Bejerano, G. (2010). GREAT improves functional interpretation of *cis*-regulatory regions. Nat. Biotechnol. *28*, 495–501.

17. Chrzanowska-Wodnicka, M., Kraus, A.E., Gale, D., White, G.C., 2nd, and Vansluys, J. (2008). Defective angiogenesis, endothelial migration, proliferation, and MAPK signaling in Rap1b-deficient mice. Blood *111*, 2647–2656.

18. Kawasaki, K., Watabe, T., Sase, H., Hirashima, M., Koide, H., Morishita, Y., Yuki, K., Sasaoka, T., Suda, T., Katsuki, M., et al. (2008). Ras signaling directs endothelial specification of VEGFR2^{+} vascular progenitor cells. J. Cell Biol. *181*, 131–141.

19. Pataskar, A., Jung, J., Smialowski, P., Noack, F., Calegari, F., Straub, T., and Tiwari, V.K. (2016). NeuroD1 reprograms chromatin and transcription factor landscapes to induce the neuronal program. EMBO J. *35*, 24–45.

20. Goode, D.K., Obier, N., Vijayabaskar, M.S., Lie-A-Ling, M., Lilly, A.J., Hannah, R., Lichtinger, M., Batta, K., Florkowska, M., Patel, R., et al. (2016). Dynamic gene regulatory networks drive hematopoietic specification and differentiation. Dev. Cell *36*, 572–587.

21. Pattabiraman, D.R., Bierie, B., Kober, K.I., Thiru, P., Krall, J.A., Zill, C., Reinhardt, F., Tam, W.L., and Weinberg, R.A. (2016). Activation of PKA leads to mesenchymal-to-epithelial transition and loss of tumor-initiating ability. Science *351*, aad3680.

22. Gascón, S., Murenu, E., Masserdotti, G., Ortega, F., Russo, G.L., Petrik, D., Deshpande, A., Heinrich, C., Karow, M., Robertson, S.P., et al. (2016). Identification and successful negotiation of a metabolic checkpoint in direct neuronal reprogramming. Cell Stem Cell *18*, 396–409.

23. Saxena, S., Rönn, R.E., Guibentif, C., Moraghebi, R., and Woods, N.B. (2016). Cyclic AMP signaling through Epac axis modulates human hemogenic endothelium and enhances hematopoietic cell generation. Stem Cell Reports *6*, 692–703.

24. Namkoong, S., Kim, C.-K., Cho, Y.-L., Kim, J.-H., Lee, H., Ha, K.-S., Choe, J., Kim, P.H., Won, M.H., Kwon, Y.G., et al. (2009). Forskolin increases angiogenesis through the coordinated cross-talk of PKA-dependent VEGF expression and Epac-mediated PI3K/Akt/eNOS signaling. Cell. Signal. *21*, 906–915.

25. Taylor, S.S., Ilouz, R., Zhang, P., and Kornev, A.P. (2012). Assembly of allosteric macromolecular switches: lessons from PKA. Nat. Rev. Mol. Cell Biol. *13*, 646–658.

26. Zeng, H., Qin, L., Zhao, D., Tan, X., Manseau, E.J., Van Hoang, M., Senger, D.R., Brown, L.F., Nagy, J.A., and Dvorak, H.F. (2006). Orphan nuclear receptor TR3/Nur77 regulates VEGF-A-induced angiogenesis through its transcriptional activity. J. Exp. Med. *203*, 719–729.

27. Licht, A.H., Pein, O.T., Florin, L., Hartenstein, B., Reuter, H., Arnold, B., Lichter, P., Angel, P., and Schorpp-Kistner, M. (2006). JunB is required for endothelial cell morphogenesis by regulating core-binding factor β. J. Cell Biol. *175*, 981–991.

28. Yamamizu, K., Matsunaga, T., Uosaki, H., Fukushima, H., Katayama, S., Hiraoka-Kanie, M., Mitani, K., and Yamashita, J.K. (2010). Convergence of Notch and β-catenin signaling induces arterial fate in vascular progenitors. J. Cell Biol. *189*, 325–338.

29. Sahara, M., Hansson, E.M., Wernet, O., Lui, K.O., Später, D., and Chien, K.R. (2014). Manipulation of a VEGF-Notch signaling circuit drives formation of functional vascular endothelial progenitors from human pluripotent stem cells. Cell Res. *24*, 820–841.

30. Welten, S.M., Bastiaansen, A.J., de Jong, R.C., de Vries, M.R., Peters, E.A., Boonstra, M.C., Sheikh, S.P., La Monica, N., Kandimalla, E.R., Quax, P.H., and Nossent, A.Y. (2014). Inhibition of 14q32 microRNAs miR-329, miR-487b, miR-494, and miR-495 increases neovascularization and blood flow recovery after ischemia. Circ. Res. *115*, 696–708.

31. Rao, X., Zhong, J., Zhang, S., Zhang, Y., Yu, Q., Yang, P., Wang, M.H., Fulton, D.J., Shi, H., Dong, Z., et al. (2011). Loss of methyl-CpG-binding domain protein 2 enhances endothelial angiogenesis and protects mice against hind-limb ischemic injury. Circulation *123*, 2964–2974.

32. Hussein, K.H., Park, K.M., Kang, K.S., and Woo, H.M. (2016). Heparin-gelatin mixture improves vascular reconstruction efficiency and hepatic function in bioengineered livers. Acta Biomater. *38*, 82–93.

33. Sumanas, S., and Choi, K. (2016). ETS transcription factor ETV2/ER71/Etsrp in hematopoietic and vascular development. Curr. Top. Dev. Biol. *118*, 77–111.

34. Wythe, J.D., Dang, L.T., Devine, W.P., Boudreau, E., Artap, S.T., He, D., Schachterle, W., Stainier, D.Y., Oettgen, P., Black, B.L., et al. (2013). ETS factors regulate Vegf-dependent arterial specification. Dev. Cell *26*, 45–58.

35. Fukuhara, S., Sakurai, A., Sano, H., Yamagishi, A., Somekawa, S., Takakura, N., Saito, Y., Kangawa, K., and Mochizuki, N. (2005). Cyclic AMP potentiates vascular endothelial cadherin-mediated cell-cell contact to enhance endothelial barrier function through an Epac-Rap1 signaling pathway. Mol. Cell. Biol. *25*, 136–146.

36. Chrzanowska-Wodnicka, M. (2017). Rap1 in endothelial biology. Curr. Opin. Hematol. *24*, 248–255.

37. Kabir, A.U., Lee, T.J., Pan, H., Berry, J.C., Krchma, K., Wu, J., Liu, F., Kang, H.K., Hinman, K., Yang, L., et al. (2018). Requisite endothelial reactivation and effective siRNA nanoparticle targeting of *Etv2/Er71* in tumor angiogenesis. JCI Insight *3*, 97349.

38. Park, C., Lee, T.J., Bhang, S.H., Liu, F., Nakamura, R., Oladipupo, S.S., Pitha-Rowe, I., Capoccia, B., Choi, H.S., Kim, T.M., et al. (2016). Injury-mediated vascular regeneration requires endothelial ER71/ETV2. Arterioscler. Thromb. Vasc. Biol. *36*, 86–96.

39. Harding, A., Cortez-Toledo, E., Magner, N.L., Beegle, J.R., Coleal-Bergum, D.P., Hao, D., Wang, A., Nolta, J.A., and Zhou, P. (2017). Highly efficient differentiation of endothelial cells from pluripotent stem cells requires the MAPK and the PI3K pathways. Stem Cells *35*, 909–919.

40. Patsch, C., Challet-Meylan, L., Thoma, E.C., Urich, E., Heckel, T., O'Sullivan, J.F., Grainger, S.J., Kapp, F.G., Sun, L., Christensen, K., et al. (2015). Generation of vascular endothelial and smooth muscle cells from human pluripotent stem cells. Nat. Cell Biol. *17*, 994–1003.

41. Prasain, N., Lee, M.R., Vemula, S., Meador, J.L., Yoshimoto, M., Ferkowicz, M.J., Fett, A., Gupta, M., Rapp, B.M., Saadatzadeh, M.R., et al. (2014). Differentiation of human pluripotent stem cells to cells similar to cord-blood endothelial colony-forming cells. Nat. Biotechnol. *32*, 1151–1157.

42. Simons, M., Gordon, E., and Claesson-Welsh, L. (2016). Mechanisms and regulation of endothelial VEGF receptor signalling. Nat. Rev. Mol. Cell Biol. *17*, 611–625.

43. Hou, P., Li, Y., Zhang, X., Liu, C., Guan, J., Li, H., Zhao, T., Ye, J., Yang, W., Liu, K., et al. (2013). Pluripotent stem cells induced from mouse somatic cells by small-molecule compounds. Science *341*, 651–654.

44. Fritz, A.L., Adil, M.M., Mao, S.R., and Schaffer, D.V. (2015). cAMP and EPAC signaling functionally replace OCT4 during induced pluripotent stem cell reprogramming. Mol. Ther. *23*, 952–963.

45. Smith, D.K., Yang, J., Liu, M.L., and Zhang, C.L. (2016). Small molecules modulate chromatin accessibility to promote NEUROG2-mediated fibroblast-to-neuron reprogramming. Stem Cell Reports *7*, 955–969.

46. Camarena, V., Sant, D.W., Huff, T.C., Mustafi, S., Muir, R.K., Aron, A.T., Chang, C.J., Renslo, A.R., Monje, P.V., and Wang, G. (2017). cAMP signaling regulates DNA hydroxymethylation by augmenting the intracellular labile ferrous iron pool. eLife *6*, e29750.

YMTHE, Volume *28*

Supplemental Information

cAMP/EPAC Signaling Enables ETV2 to Induce Endothelial Cells with High Angiogenesis Potential

Jae-Jun Kim, Da-Hyun Kim, Jin Young Lee, Byung-Chul Lee, Insung Kang, Myung Geun Kook, Dasom Kong, Soon Won Choi, Heung-Myong Woo, Dong-Ik Kim, and Kyung-Sun Kang

SUPPLEMENTAL INFORMATION

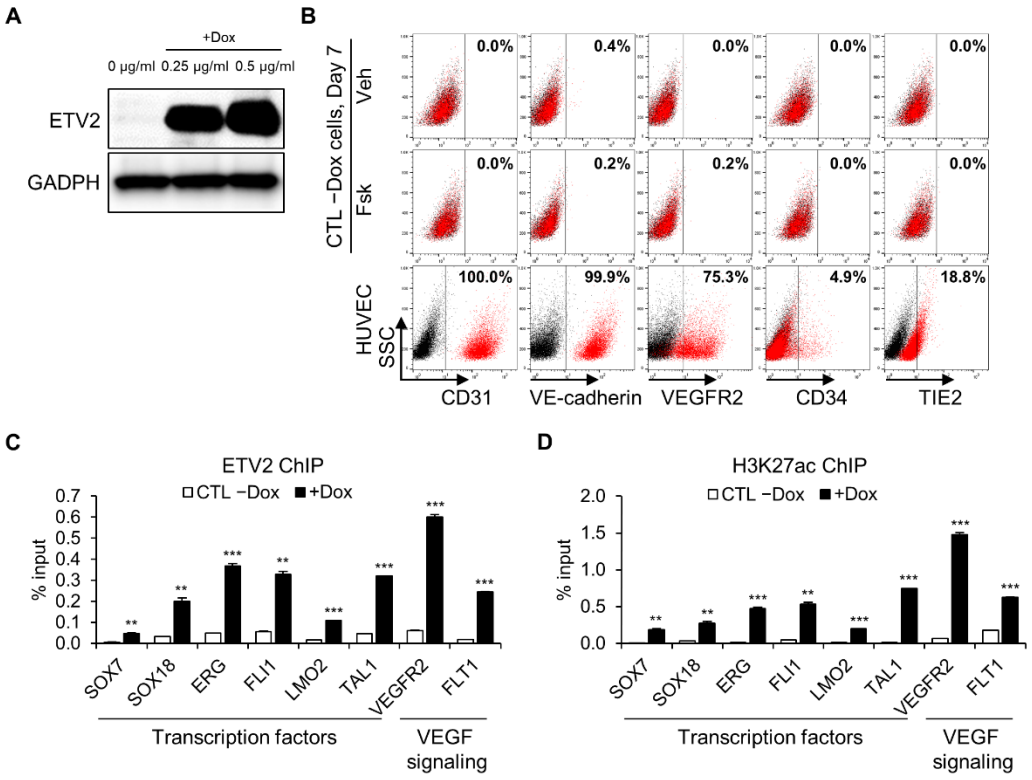

Figure S1, related to Figure 1. Establishment and characterization of ETV2-expressing hDFs.

(A) Western blot analysis of ETV2 expression in ETV2-hDFs 3 days after treatment with the indicated concentrations of doxycycline. (B) FACS analysis of CD31, VE-cadherin, VEGFR2, CD34 and TIE2 expression in ETV2-hDFs without doxycycline treatment and HUVECs. (C and D) ChIP-qPCR results showing enrichment of ETV2 (C) and H3K27ac (D) at genomic loci of indicated genes. Target genes were associated with ETV2-bound promoters (*SOX18*, *TAL1*, and *FLT1*) or with ETV2-bound enhancers (*SOX7*, *ERG*, *FLI1*, *LMO2*, *TAL1*, and *VEGFR2*). Each group n=3, mean ±SD, **p < 0.01 ***p < 0.001 versus CTL –Dox.

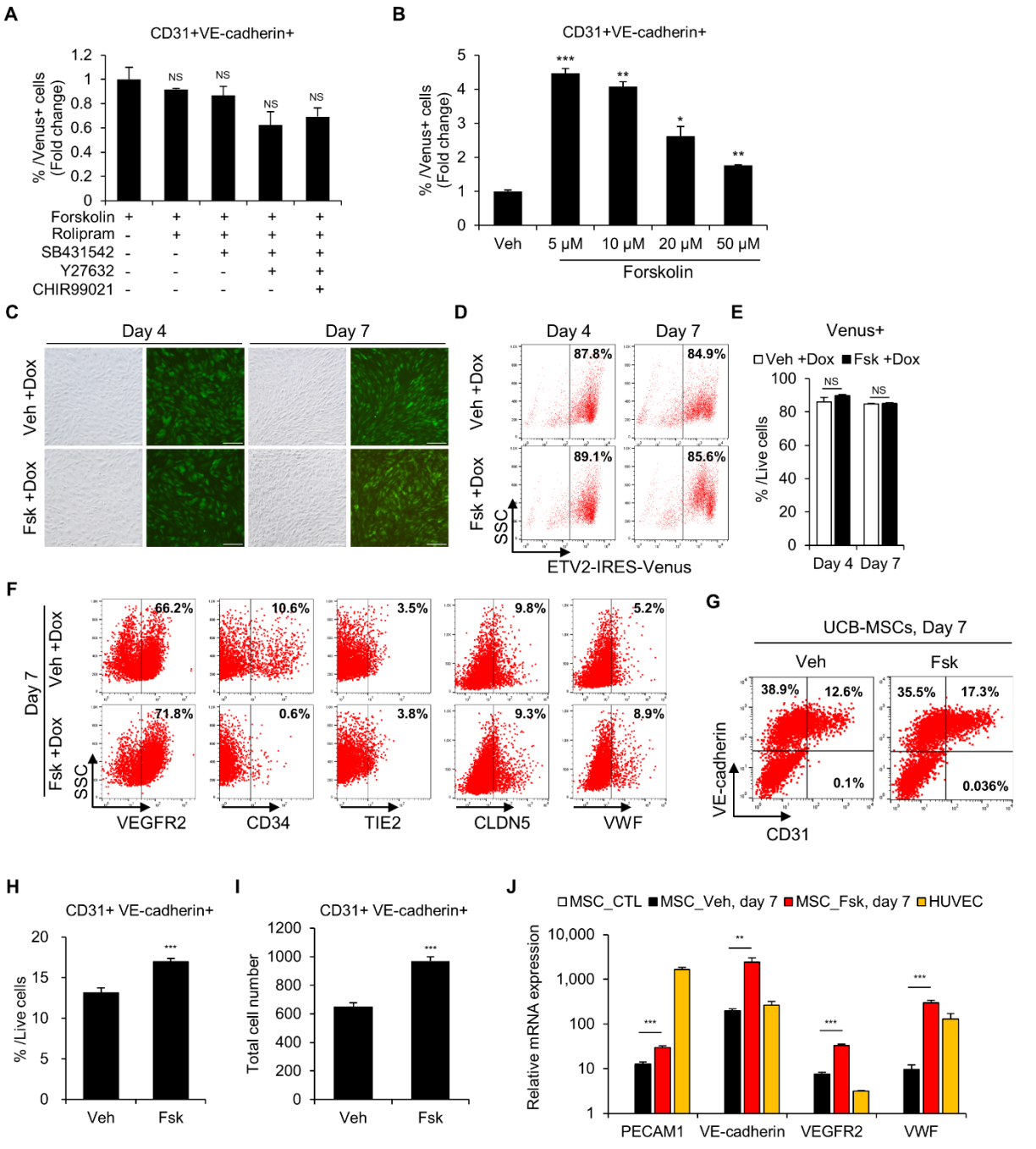

Figure S2, related to Figure 2. Forskolin enhances the efficiency of iEC reprogramming.

(A) Quantification of the averaged percent iECs (from the flow cytometry analysis) at day 10 after adding individual small molecules to the forskolin treatment. Data are shown as the mean ±SD. (B) Concentration of forskolin was titrated during iEC reprogramming by flow cytometry analysis. Each group, n=3. Data are shown as the mean ±SD. *p < 0.05 **p < 0.01 ***p < 0.001 versus Vehicle. (C) Phase-contrast images and ETV2-Venus fluorescence images

of ETV2-hDFs on day 4 and 7 of induction. Scale bar, 200 μm. (D and E) FACS analysis results (D) and quantification (E) showing ETV2-IRES-Venus+ populations at day 4 and 7 with dox treatment. (F) Representative FACS results of iECs at day 7 of dox treatment. The expression of VEGFR2, CD34, TIE2, CLDN5, and VWF were presented after gating on the Venus+ populations. (G-I) Representative FACS profiles (G) and quantification (H and I) of UCB-MSCs transduced with retroviral ETV2 on day 7 of induction. Each group, n=3, mean ±SD, ***$p < 0.001$ versus Vehicle. (J) qRT-PCR analysis of *PECAM1* and *VE-cadherin, VEGFR2 and VWF* in iECs derived from UCB-MSCs after treatment with forskolin on day 7 of induction. Each group, n=3, mean ±SD, **$p < 0.01$ ***$p < 0.001$ versus Vehicle.

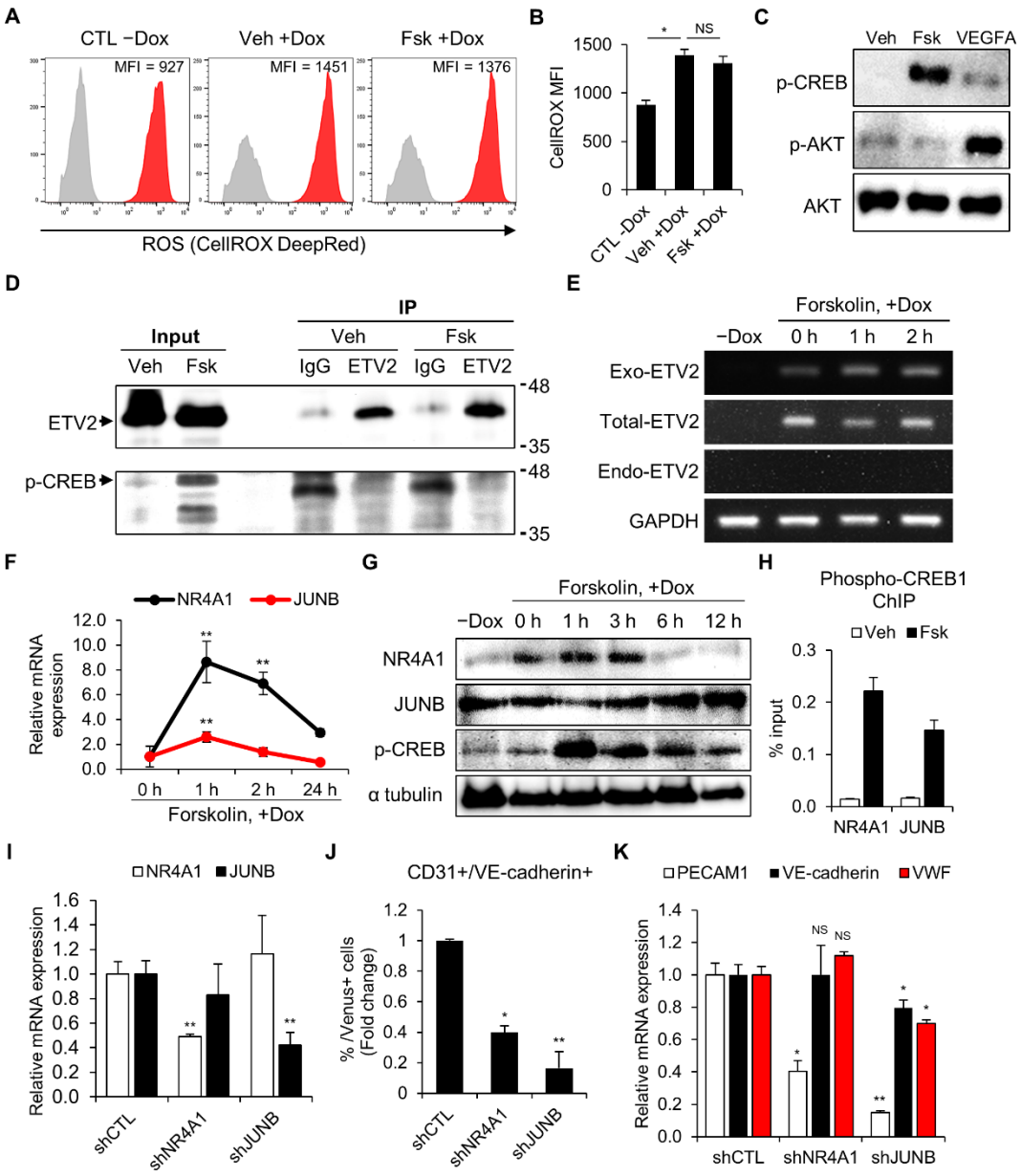

Figure S3, related to Figure 3. The independence of ETV2 and p-CREB in iEC reprogramming.

(A and B) Representative FACS profiles (A) and quantification (B) of CTL −Dox, Veh +Dox, and Fsk +Dox loaded with ROS-indicator CellROX DeepRed on day 7 of induction. Gray histograms indicate cells without CellROX treatment. Each group, n=3. Data are shown as the mean ±SD. *p < 0.05. NS, not statistically significant. (C) Western blot analysis of phospho-CREB, phospho-AKT, and total AKT levels after the indicated treatments in +Dox cells starved for 4 hr. (D) Co-immunoprecipitation analysis of ETV2 and p-CREB protein interactions. ETV2-hDFs were treated with Veh or Fsk for 1 hour after day 7 of induction, and cell extracts were immunoprecipitated with anti-ETV2

or non-immune IgG. (E) RT-PCR analysis of exogenous (exo-ETV2), total, and endogenous ETV2 (endo-ETV2) expression in ETV2-hDFs without or with dox for 7 days. Cells were treated with vehicle or forskolin for the indicated lengths of time. (F) qRT-PCR analysis of *NR4A1* and *JUNB*, related to vasculature development as well as putative CREB targets, in iECs after treatment with forskolin for the indicated lengths of time. Each group, n=3. All data are shown as the mean ±SD. **p < 0.01 versus Vehicle. (G) Immunoblot for NR4A1, JUNB and phospho-CREB in control cells without dox and iECs after treatment with forskolin for the indicated lengths of time. (H) Chromatin immunoprecipitation qPCR analysis of phospho-CREB occupancy on *NR4A1* and *JUNB* in iECs treated with vehicle or forskolin for 1 hour. Each group, n=3. Values (% of inputs) are presented as the mean ±SD. (I) qRT-PCR validation for silencing of *NR4A1* and *JUNB* in iECs transduced with each shRNA. Each group, n=3. All data are shown as the mean ±SD. **p < 0.01 versus shCTL. (J) FACS analysis of CD31+/VE-cadherin+ population in iECs transduced with shCTL, shNR4A1 and shJUNB on day 10 of induction. Each group, n=3. All data are shown as the mean ±SD. *p < 0.05 **p < 0.01 versus shCTL. (K) qRT-PCR analysis of *PECAM1*, *VE-cadherin*, and *VWF* in iECs transduced with shCTL, shNR4A1 and shJUNB on day 7 of induction. Each group, n=3. All data are shown as the mean ±SD. *p < 0.05 **p < 0.01 versus shCTL. NS, not statistically significant.

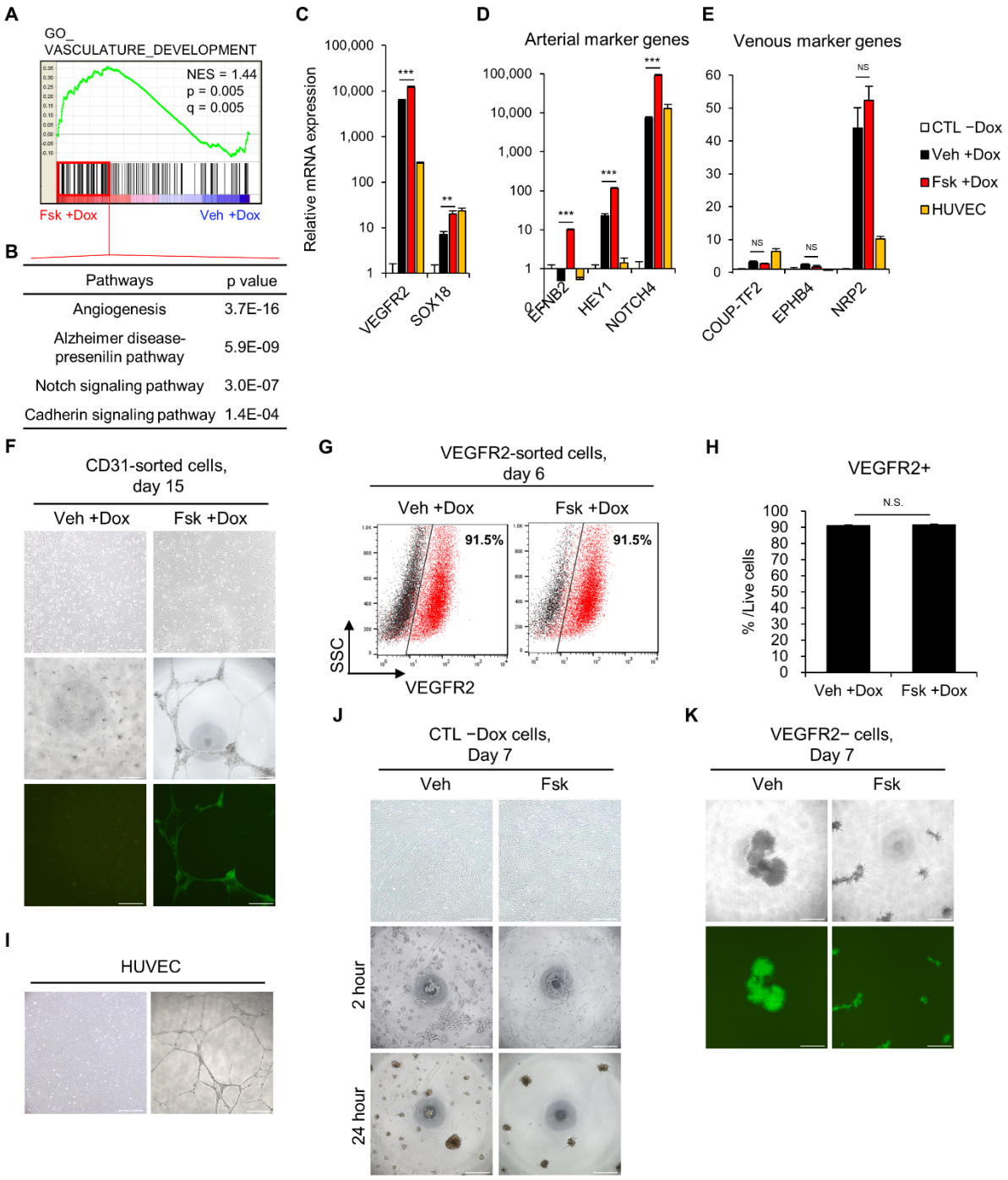

Figure S4, related to Figure 4. Forskolin preferentially induces arterial markers expression and enhances angiogenesis during iEC reprogramming.

(A and B) GSEA was performed comparing transcriptional profiles from Veh +Dox and Fsk +Dox. The enrichment score plots show a positive correlation of Fsk +Dox relative to Veh +Dox in the vasculature development (A). Top

pathways associated with leading edge genes which significantly contribute to the enrichment of the vasculature development gene set in Fsk +Dox (B). (C-E) qRT-PCR of vasculature development genes (C), arterial marker genes (D) and venous marker genes (E) in CTL −Dox, Veh +Dox, Fsk +Dox, and HUVECs on day 7 of induction. Each group, n=3. All data are shown as the mean ±SD. **$p < 0.01$ ***$p < 0.001$ versus Veh +Dox. NS, not statistically significant. (F) Phase-contrast images (top) of CD31-sorted cells from ETV2-hDFs on day 14 of induction. Representative phase-contrast images (middle) and ETV2-Venus fluorescence images (bottom) of tubular structures 24 hours after plating on Matrigel. Scale bar, 500 μm. (G-H) Representative FACS profiles (G) and quantification (H) of VEGFR2 in VEGFR2-sorted cells at day 6 post-induction. Each group, n=3. Data are shown as the mean ±SD. NS, not statistically significant. (I) Phase-contrast image of HUVECs showing the formation of lumen-like structure. Scale bar, 500 μm. (J) Phase-contrast images (top) of CTL −Dox cells on day 7 of indicated treatments. Representative phase-contrast images of CTL −Dox cells 2 hours (middle) and 24 hours (bottom) after embedding in Matrigel. Scale bar, 500 μm. (K) Representative phase-contrast images (top) and ETV2-Venus fluorescence images (bottom) of VEGFR2-negative cells 24 hours after plating on Matrigel. Scale bar, 500 μm.

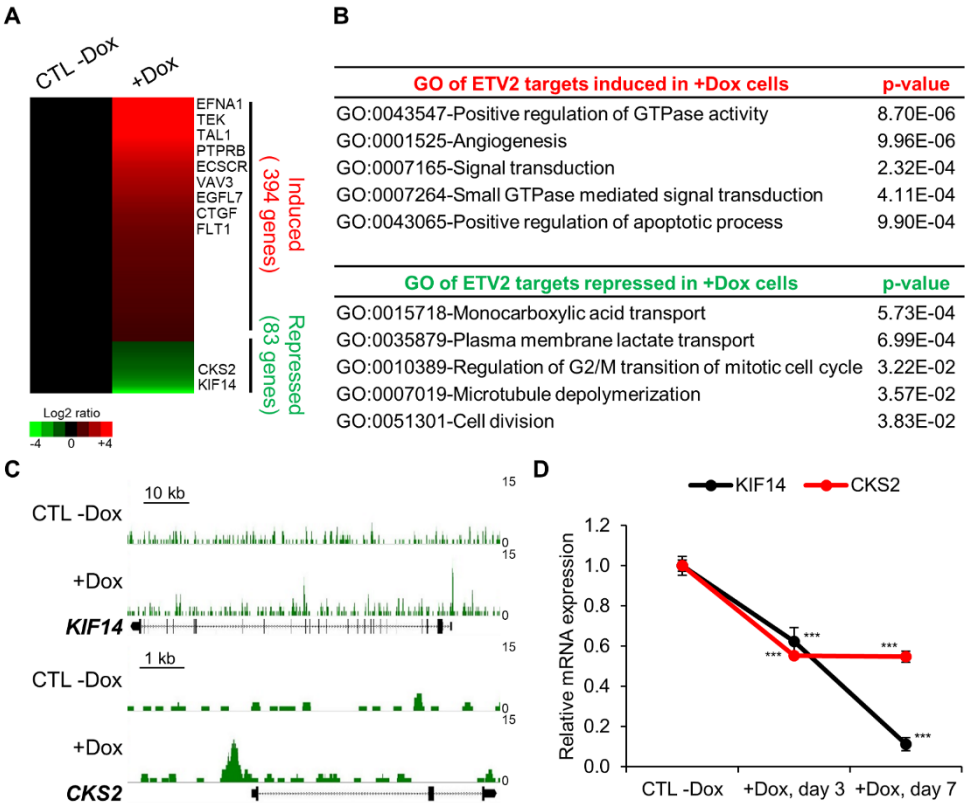

Figure S5, related to Figure 6. ETV2 directly regulates angiogenesis- and cell cycle-related genes.

(A) Heatmap representing the log-fold expression changes of promoter-bound ETV2 target genes (477 genes) during endothelial reprogramming (at day 7 of dox treatment). The overlap between differentially expressed genes (≥2-fold between CTL −Dox and +Dox group) and genes with ETV2 occupancy within the promoter region were presented. (B) Gene ontology terms of promoter-bound ETV2 target genes that are induced or repressed during endothelial reprogramming analyzed by DAVID functional annotation tool. (C) IGB track displaying ETV2 ChIP-seq signal in promoter region of *KIF14* (upper) *and CKS2* (lower). (D) qRT-PCR analysis of *KIF14* and *CKS2*, ETV2 target genes, in ETV2-hDFs without or with doxycycline treatment on day 3 and 7 of induction. Each group, n=3. All data are shown as the mean ±SD. ***p < 0.001 versus CTL −Dox.

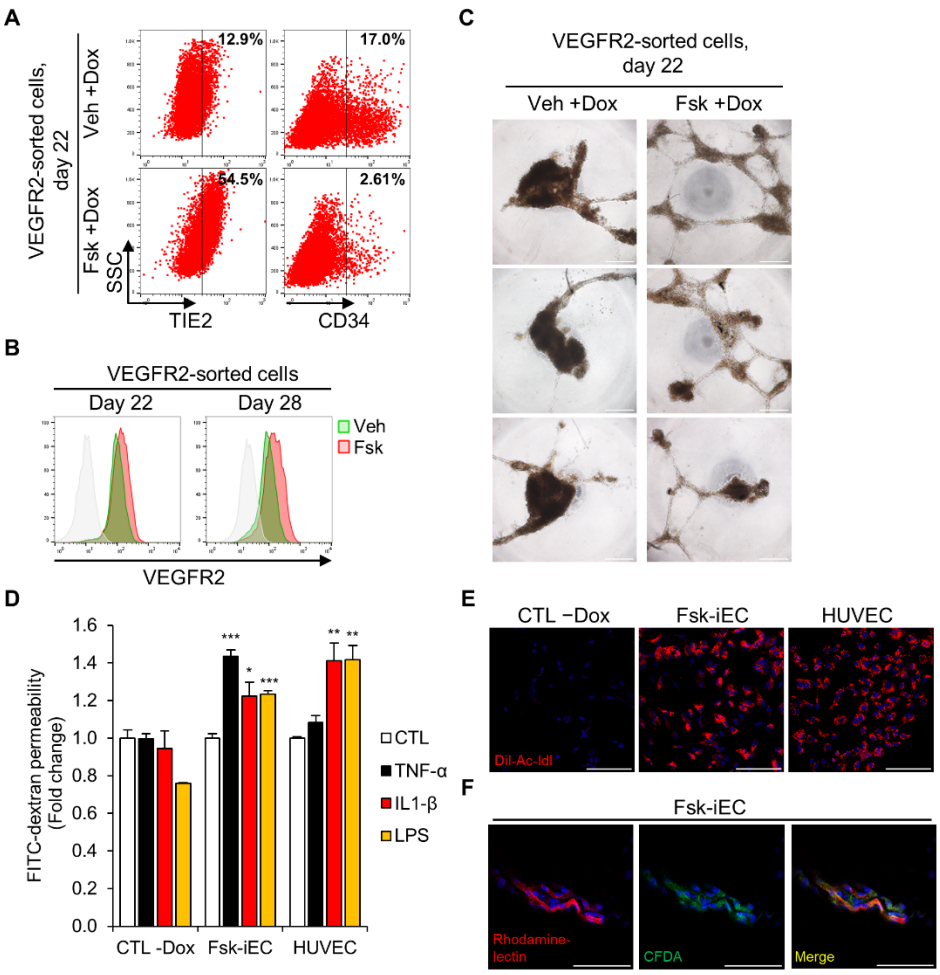

Figure S6, related to Figure 6. Fsk-iECs have functional characteristics *in vitro* and *in vivo*.

(A) Representative flow cytometry analysis in VEGFR2-sorted iECs treated with vehicle or forskolin at day 22 of induction. (B) Representative FACS profiles of VEGFR2 in VEGFR2-sorted iECs treated with vehicle or forskolin at day 22 and 28 of post-induction. (C) Representative phase-contrast images of tubular structures 24 hours after plating on Matrigel. 30,000 cells were applied for each assay (in triple replication). Scale bar, 500 μm. (D) FITC-dextran permeability assays in Fsk-iECs and HUVECs. Quantification of increased permeability in response to a 24-hours exposure to various inflammatory cytokines including TNF-α, IL1-β, or LPS. Each group, n=4. All data are shown as the mean ±SD. *$p < 0.05$ **$p < 0.01$ ***$p < 0.001$ versus CTL. (E) Representative fluorescence images demonstrating DiI-acetylated-low density lipoprotein (DiI-Ac-ldl, red) uptake in Fsk-iECs and HUVECs. Nuclei were counter-stained with DAPI (blue). Scale bar, 100 μm. (F) High magnification confocal micrograph showing co-localization of rhodamine-lectin-labeled blood vessels (red) and CFDA-labeled Fsk-iECs (green). Nuclei were counter-stained with DAPI (blue). Matrigel-embedded Fsk-iECs were subcutaneously injected into the flanks of Balb/c nude mice. On day 14 post-injection, the mice were intravenously perfused with rhodamine-isolectin before sacrifice. Scale bar, 60 μm.

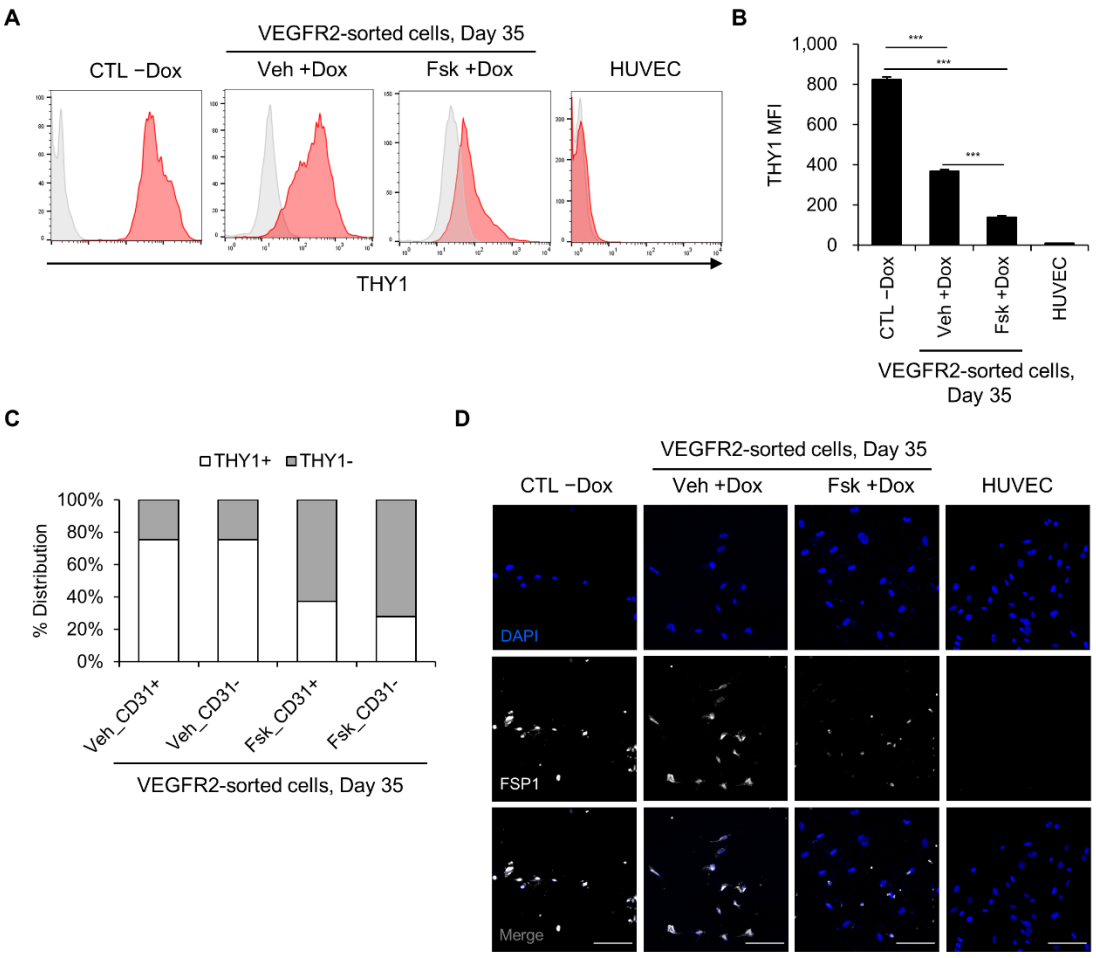

Figure S7, related to Figure 6. Forskolin treatment reduces mesenchymal phenotypes during endothelial reprogramming in long-term cultures.

(A and B) Representative FACS profiles (A) and quantification of MFI (B) of THY1 in CTL −Dox, Veh +Dox, Fsk +Dox and HUVECs on day 35 of induction. Gray histograms indicate non-stained controls. Each group, n=3. Data are shown as the mean ±SD, ***$p < 0.001$. (C) FACS analysis of Veh +Dox and Fsk +Dox after co-staining of THY1 and CD31 on day 35 of induction. Distribution of THY1+ or THY1- cells were analyzed among CD31+ populations and CD31- populations respectively. (D) Representative confocal microscopic images of CTL −Dox, Veh +Dox, Fsk +Dox and HUVECs on day 35 of induction. The cells of each group were stained with FSP1 (white) and nuclei were counter-stained with DAPI (blue). Scale bar, 100 μm.

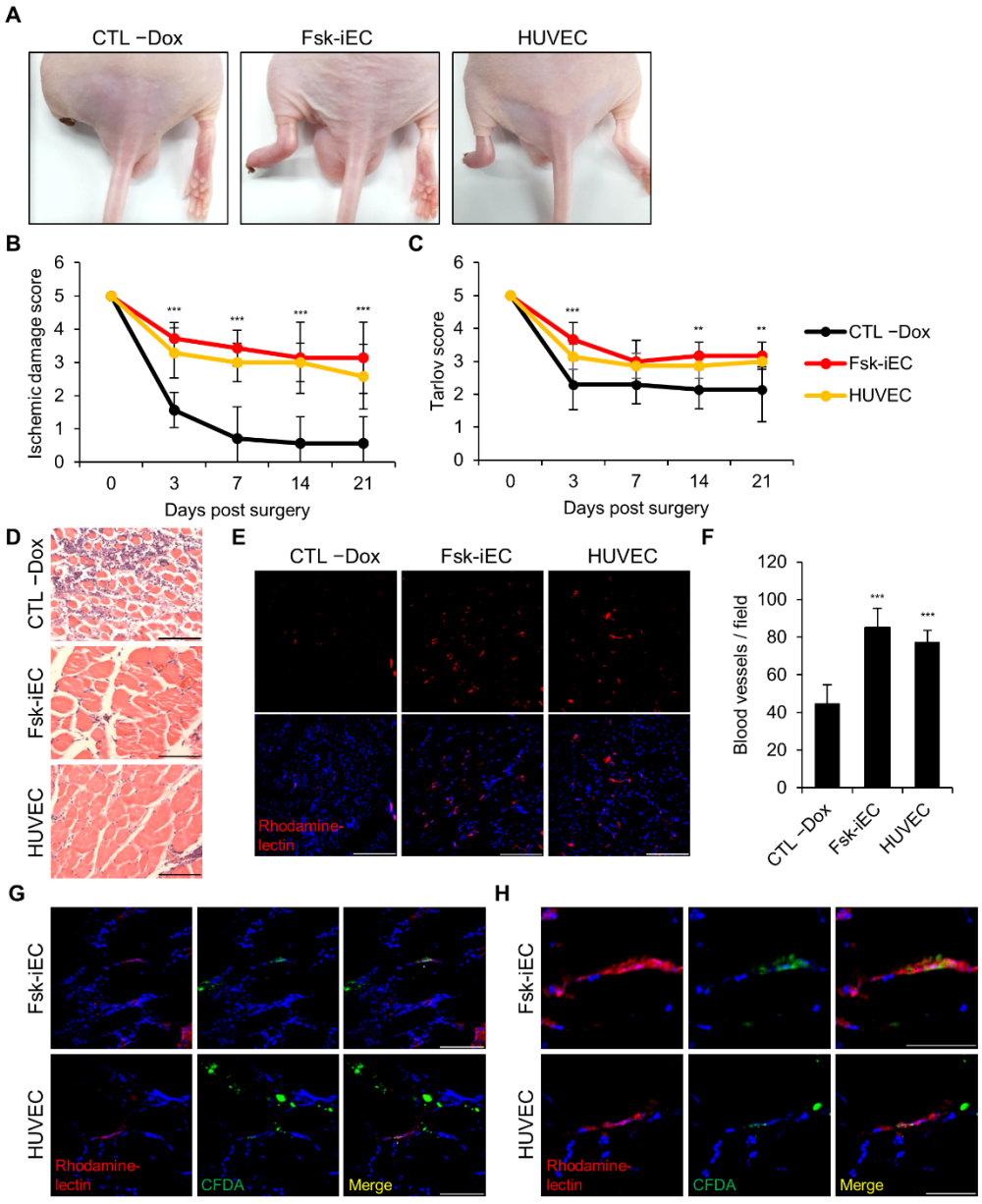

Figure S8, related to Figure 6. Fsk-iECs have therapeutic efficacy in severe hindlimb ischemia model.

(A) Representative images of mouse ischemic hindlimbs at day 21 treated as indicated. (B and C) Ischemic damage scores (B) and Tarlov scores (C) were monitored at the indicated times following injection of CTL −Dox, Fsk-iEC, and HUVEC into ischemic hindlimbs. n=7, 6, and 7, respectively. Data are shown as the mean ±SD. **p < 0.01 ***p < 0.001. CTL −Dox versus Fsk-iEC by two-way ANOVA. (D) Representative H&E stained sections of ischemic muscles from CTL −Dox, Fsk-iEC, and HUVEC-treated mice on day 21 postsurgery. Scale bar, 200 μm. (E and F) Representative immunofluorescence images (E) and quantification (F) of rhodamine-lectin-stained blood vessels (red)

in the hindlimb muscle sections on day 21 postsurgery. Nuclei were counter-stained with DAPI (blue). Scale bar, 200 μm. Each group, n=11. Data are shown as the mean ±SD. ***$p < 0.001$ versus CTL −Dox. (G) Representative confocal microscopic images on day 21 post transplantation of CFDA-labeled Fsk-iECs and HUVECs. White arrows indicate labeled cells (green) which are incorporated into lectin-positive (red) vessels. Nuclei were counter-stained with DAPI (blue). Scale bar, 100 μm. (H) Magnified confocal microscopic images of localized Fsk-iECs and HUVECs in blood vessels shown in (G). Scale bar, 50 μm.

Table S1. Representative signaling pathways of ETV2 target genes in human fibroblasts from KEGG pathway analysis, related to Figure 1.

Rap1 signaling pathway	F2RL3	ADCY1	PDGFB	PDGFA	EFNA1	CSF1
	BCAR1	KITLG	ITGB2	KIT	RASGRP3	P2RY1
	RASGRP2	TEK	RAPGEF5	RAPGEF3	RAPGEF2	FGF1
	THBS1	PIK3R3	MAP2K6	PARD6A	FLT1	FLT4
	SIPA1L2	MAPK11	KDR	DOCK4	LAT	PLCG1
	LPAR5	ARAP3	F2R	NGF		
PI3K-Akt signaling pathway	PDGFB	PDGFA	EFNA1	CSF1	COL3A1	ITGA11
	KITLG	NFKB1	KIT	CCNE2	CCNE1	IL4R
	COL27A1	TEK	COL6A1	PIK3R3	FGF1	THBS1
	GHR	COL4A2	FLT1	COL4A1	FLT4	TP53
	ITGA1	CREB5	COL5A2	COL5A1	BCL2L11	KDR
	LAMA2	VWF	LPAR5	CCND2	LPAR6	ITGA8
	COL1A2	F2R	NGF			
Ras signaling pathway	PLD1	FLT1	PDGFA	EFNA1	CSF1	KITLG
	NFKB1	KIT	KDR	LAT	RASA4B	PLCG1
	RASGRP3	GAB1	TEK	RASGRP2	RAPGEF5	FGF1
	PIK3R3	PLA2G4C	RASA4	NGF		
MAPK signaling pathway	MEF2C	PDGFB	PDGFA	NFKB1	TGFB2	MAX
	HSPA2	RASGRP3	ELK4	MAP3K1	RASGRP2	RAPGEF2
	MAPK11	ARRB1	GADD45G	HSPB1	PLA2G4C	NGF
	DUSP6	MAP3K11	FGF1	MAP2K6	CACNA2D1	NTF3
	TGFBR1	TP53				

Table S2. Small-molecule compounds used for screening in endothelial reprogramming, related to Figure 2.

Name	Function	Concentration (μM)
SB203580	p38 MAPK inhibitor	20
Salirasib	Ras inhibitor	25
LY294002	PI3K inhibitor	5
SP600125	JNK inhibitor	2
Y-27632	ROCK inhibitor	10
DAPT	NOTCH inhibitor	10
CHIR99021	GSK3 inhibitor	10
SB431542	TGFβ inhibitor	5
Rolipram	PDE4 inhibitor	2
Forskolin	PKA and EPAC activator	10

Table S3. Leading edge genes from GSEA associated with pathways, related to Figure 4.

Angiogenesis	PIK3CG	FZD8	PDGFB	JAG1	PTPRB	TEK
	EPHB1	NOTCH4	RHOB	ANGPT2	NOTCH1	PDGFA
	FZD5	KDR				
Alzheimer disease-presenilin pathway	FZD8	FZD4	PCSK5	ACTA2	FZD5	NOTCH4
	NOTCH3	NOTCH1				
Notch signaling pathway	HES1	JAG1	NOTCH4	NOTCH1	NOTCH3	
Cadherin signaling	FZD8	FZD4	ACTA2	FZD5	CDH5	

Table S4. List of primers used for RT-PCR, qRT-PCR and ChIP-qPCR, related to Figure 1, 2, and 3.

Genes	5'-Forward sequence-3'	5'-Reverse sequence-3'
GAPDH	TGATGACATCAAGAAGGTGGTG	ACCCTGTTGCTGTAGCCAAAT
PECAM1	AGCAGCATCGTGGTCAACATAAC	GCAGGACAGGTTCAGTCTTTCA
VE-cadherin	CTTCACCCAGACCAAGTACACA	AATGGTGAAAGCGTCCTGGT
VWF	CGTGGTCCTGAAGCAGACATA	TTGCTGCTGGTGAGGTCATT
VEGFR2	CGGTCAACAAAGTCGGGAGA	CAGTGCACCACAAAGACACG
RAPGEF3	TGGGACGTTGTGTGCAATAG	ACACGGTACACACATGCAG
RAP1A	AAGAACGGCCAAGGTTTTGC	CTTCCGTGTCCTTAACCCGT
RAP1B	GATTCAGGCGTGTAAACCAGC	CGAACCTCTCACGCTGTCA
EFNB2	AAGGACTGGTACTATACCCACAG	TGTCTGCTTGGTCTTTATCAACC
HEY1	AAATGCTGCATACGGCAGGA	ATAACGCGCAACTTCTGCCA
NOTCH4	ACTCTCTGGCCAATGCCTTC	TTCAAAACCCTTGGGGCAGT
COUP-TF2	CGGATCTTCCAAGAGCAAGTG	ACAGGCATCTGAGGTGAACAG
EPHB4	CCACCGGGAAGGTGAATGTC	CTGGGCGCACTTTTTGTAGAA
NRP2	AGCCCTGTGGTTGGATGTATGA	ACTCTGCAGCCGCAAGAAAT
NR4A1	TGCCAATCTCCTCACTTCCCT	CCAGCATCTTCCTTCCCAAAG
JUNB	GTGCCGAAAAAGGAAGCTGG	CTGCGTTAGCATGAGTTGGC
KIF14	GTCCAAAGAAGAGCTTAGGGT	TACTGTGGGTGAGGGCATTC
CKS2	GGCTGGACGTGGTTTTGTCT	ATGCCGGTACTCGTAGTGTTC
SOX18	CCTCACCGAGTTCGACCAG	ATGCACGCGCTGTAATAGAC
FOXO1	GGGCAACCTGTCCTACGC	TCTTGCCACCCTCTGGATTG
TSPAN12	CCTGTGGTTCATCCGGTCAT	CGCCACAAGCCAGTTCTACA
EDN1	GGAGCTGTTTACCCCCACTCT	GATCCTTCAGCCCAAGTGCC
NGFR	AGTCAGGTTTGGGGTTCGTG	GTTAGCTCCGGGTCCATGTC
SNAI2	ATCACTGTGTGGACTACCGC	TCACTCGCCCCAAAGATGAG
TWIST1	TCTCAAGAGGTCGTGCCAATC	TGACTATGGTTTTGCAGGCCA
Exogenous *ETV2*	CCATATGATGTTCCAGATTATGC	ACTTCTGGGTGCAGTAACG
Total *ETV2*	AGCTGGCAGGGCTTGAAGG	CAGGGATGAGCTTGTACCTTTCCA
Endogenous *ETV2*	CATGTCGCAGGATCGAGACC	GCCTTCTGAATGTTCTCTGGC
SOX7 for ChIP-qPCR	CCGGAGCGAGCTAATCTGGA	CCCAGTGTTTCCTGCCTGAT
SOX18 for ChIP-qPCR	GTTCCATGGGAAGCAGGCTGGG	GGCCTTCCTTCCTGAGCTGCA
ERG for ChIP-qPCR	GGGCTGGCTATCTGTGTAGGAAG	GCTGCTACAGCAATTACCTTGAGGA
FLI1 for ChIP-qPCR	GACTTCAGGCTCCAGTTTCTCTTGA	AAAGGAACTGGTGTGAGGCAGCTTT
LMO2 for ChIP-qPCR	GCTTCCTCCTCTCTCGGGAAGGTCTA	ACCGGGCAGCTGTCTCTTTAA
TAL1 for ChIP-qPCR	AACGGAAGCTGTGCGCTAAG	GTCACTCTCTCGTGGACGCT
VEGFR2 for ChIP-qPCR	GCCCAGCATGTCTGAACATTTAG	GACAGGAAGTAAGCGATCAGGAAATG
FLT1 for ChIP-qPCR	GGAGCAGCAATCAGAAACAGCTTT	CGGATGTGGGGAGATGTCAAGAA
*RAPGEF3*_P1 for ChIP-qPCR	GCCACAGTACAACTGCCCCAG	GTGAAGGTCTTCCTGTTCCTCCC

*RAPGEF3*_P2 for ChIP-qPCR	CAAACAAGGAAACCGGGGAGAG	GAACCGAAACAGGAGGCAGACA
Neg CTL for ChIP-qPCR	AGAGGGGAACCCACCAAATAG	AATCCCGAATGGAAAGGGGAGA
NR4A1 for ChIP-qPCR	GATCAAACAATCCGCGCTCC	GCACTCCCCCAAGTTTCGTA
JUNB for ChIP-qPCR	TGTTTACAAGGACACGCGCT	AGCCACACGCCTTTATACCG

Supplemental Methods

Cell culture

Human dermal fibroblasts, purchased from Life Technologies (C0045C), were maintained in Fibroblast Growth Medium-2 (FGM-2, Gibco). Human umbilical vein endothelial cells (HUVECs, ATCC) and human umbilical cord blood-derived mesenchymal stem cells (UCB-MSCs) were cultured in Endothelial Growth Medium-2 (EGM-2, Lonza). UCB-MSCs were isolated from human cord blood samples under approval of Institutional Review Board (IRB No. 1608/001-021) as previously described[1]. 293FT cells (Invitrogen) were cultured in Dulbecco's modified eagle medium (DMEM, high glucose, Hyclone). All medium was supplemented with 10% fetal bovine serum (FBS, Gibco) and antibiotics (100 U/ml Penicillin, 100 µg/ml Streptomycin; P/S; Gibco). Cells were maintained at 37°C in a humidified incubator with 5% CO_2.

Virus production and transduction

293FT cells were plated on 0.1% gelatin-coated 100 mm dishes 24 hours prior to transfection and maintained in fresh DMEM without Penicilin-Streptomycin (P/S). 293FT cells were transfected with following lentiviral vectors: CSII-EF-HA-ETV2-IRES-Venus, reverse tetracycline transactivator FUW-M2rtTA (#20342, Addgene). The vector CSII-EF-HA-ETV2-IRES-Venus was a generous gift from Rimpei Morita (Keio University). The constructs were co-transfected with pCMV-dR8.2 dvpr (#8455, Addgene) and pMD2.G (#12259, Addgene) for packaging into 293FT cells using FuGENE 6 (Promega). For UCB-MSCs, retroviral pMX-ETV2 was constructed. The supernatant of culture was collected twice at 48 hours and 72 hours post-transfection. Collected virus-containing medium was filtered with 0.45 µm polyvinylidene fluoride membrane (Pall Life science) and concentrated using Lenti-X Concentrator (Clontech). Concentrated virus particles were stored at -80°C or freshly used. For viral transduction, cultured cells were incubated with original growth medium containing active lentiviral particles and 5 µg/ml Polybrene (Sigma) for 24 hours.

For shRNA-mediated gene knockdown, the cells transduced with ETV2 were infected with the following shRNA constructs: pLKO.1-scramble control shRNA (#1864, Addgene), pLKO.1-shRAP1A (TRCN0000029785, Sigma) pLKO.1-shRAP1B (TRCN0000029174, Sigma), pLKO.1-shNR4A1 (TRCN0000019426, Sigma), and pLKO.1-shJUNB (TRCN0000014947, Sigma).

Generation of iECs and cell sorting

To purify CD31- or VEGFR2-positive population among total populations, immune-magnetic cell separation with microbead was performed manually following the manufacturer's instructions. Treated with doxycycline, the cells were harvested with 0.25% trypsin-EDTA (Gibco) and suspended in MACS buffer. The cells were incubated for 15 minutes at 4°C with human CD31 microbeads (CD31 MicroBead Kit, Miltenyi Biotec) or anti-human VEGFR2 antibody conjugated to biotin (130-100-308, Miltenyi Biotec). Subsequently, the cells were washed and repelleted by centrifugation. The pellet was resuspended in MACS buffer and anti-biotin microbeads (130-090-485, Miltenyi Biotec) were added for VEGFR2-positive cells purification. After incubation with microbeads for 20 minutes at 4°C, the cells were washed and subjected to cell separation using LS Columns (Miltenyi Biotec). To generate late iECs, early iECs, which were sorted by VEGFR2-positive expression on day 7, were cultured in the doxycycline-withdrawn medium until day 13. With the retreatment of doxycycline from day 14, late iECs were generated.

Flow cytometry

Cells were harvested and resuspended in PBS at 2 x 10^5 cells per 50 μL. The cells were incubated for 15 minutes with the following antibodies: PE-conjugated anti-human CD31 (555446, BD Pharmingen), Alexa Fluor 647-conjugated anti-human VE-cadherin (561567, BD Pharmingen), APC-conjugated anti-human VEGFR2 (130-098-910, Miltenyi Biotec), PE-conjugated anti-human TIE2 (FAB3131P, R&D systems), anti-human CLDN5 (35-2500, Invitrogen), anti-human VWF (555849, BD Pharmingen), PE-conjugated anti-human CD34 (555822, BD Pharmingen), APC-conjugated human THY1 (559869, BD Pharmingen). After washing with PBS, analyses were performed by FACS Calibur (BD bioscience). Data were analyzed using FlowJo software.

Immunocytochemistry

Cultured cells were fixed with 4% paraformaldehyde in PBS for 10 minutes at room temperature. After washed with PBS, the cells were permeabilized with 0.25% Triton X-100 (Sigma) for 10 minutes and blocked with 5% goat serum (Vector Laboratories) in PBS for an hour. Afterwards, the cells were incubated overnight at 4°C with the following primary antibodies: anti-human CD31 (14-0319-80, eBioscience), anti-human VE-cadherin (348502, BioLegend) and anti-human FSP1 (ab41532, Abcam). Secondary Alexa 555-labeled antibodies (Invitrogen) or Alexa 647-labeled antibodies (Invitrogen) were applied for an hour at room temperature. Nuclei were stained with 4', 6-diamidino-2-

phenylindole (DAPI, sc3598, Santa Cruz Biotechnology) for 10 minutes. Finally, the cells were mounted in fluorescent mounting medium (S302380, DAKO). Stained signals were visualized by Eclipse TE 2000 confocal laser scanning microscope (Nikon, Japan).

In vitro Matrigel tube formation assay

Basement membrane matrix (Matrigel, BD Biosciences) were plated to 96 well culture plate. After solidifying Matrigel by incubating at 37°C, a total of 2 x 10^4 cells was plated onto Matrigel-coated wells and incubated for 24 hours at 37°C in a humidified incubator with 5% CO_2. The tube formation images were captured using light microscope (IX70, Olympus).

ChIP sequencing and ChIP quantitative PCR

The cells were maintained in EGM-2 with or without doxycycline treatment for 7 days. ChIP Assay Kit (EMD Millipore) was utilized following the manufacturer's instructions. Briefly, formaldehyde was added to culture medium at a final concentration of 1% and cells were incubated for 10 minutes at 37°C. Then glycine was added at a final concentration of 125 mM to the media, followed by washing with cold PBS containing protease inhibitors twice. The cells were harvested by scraping with Farnham lysis buffer (5 mM PIPES at pH 8.0, 85 mM KCl, 0.5% NP-40) and collected by centrifugation. Cell lysates were resuspended with SDS lysis buffer and incubated for 10 minutes on ice. DNAs in lysates were sheared into 100 to 500 base pairs by sonication and sheared chromatin was purified by centrifugation (15000 x g, 4°C, 10 minutes). After calculation of DNA concentration, 1% of sheared chromatin was stored at -20°C as input. To precipitate chromatin, antibody against HA (901501, BioLegend) was added to the supernatant fraction and incubated overnight at 4°C. By incubation with Protein A Agarose/Salmon Sperm DNA for an hour, unbound DNA was removed, and HA-bound complex was collected. To reverse protein-DNA crosslinking, the solution and stored input were incubated with 5M NaCl for 4 hours at 65°C. Additionally, RNase A and Proteinase K were added and incubated for an hour at 45°C. Purified DNAs by PCR purification kit (Invitrogen) were subjected to sequencing library preparation using NEBNext® UltraTM DNA Library Prep Kit for Illumina (New England Biolabs) according to the manufacturer's instructions. The chipped DNA was ligated with adaptors. Then, after purification, PCR reaction was done with adaptor-ligated DNA and index primer. High-throughput sequencing was performed as single-end 75-bp sequencing using NextSeq 500 (Illumina).

For ChIP qPCR, cells were treated with DMSO or forskolin for the described time course. To precipitate chromatin, antibodies against H3K27ac (ab4729, Abcam) and phospho-CREB (#9198, Cell Signaling Technology) was added to the supernatant fraction and incubated overnight at 4°C. Non-specific IgG was used as negative control. Purified DNAs by PCR purification kit (Invitrogen) were subjected to PCR for amplification of DNAs bound to the precipitated complex. Quantitative real-time PCR was performed to quantify the amount of H3K27ac-bound or phospho-CREB-bound chromatin compared to that of input. The qPCR primers used for ChIP assay are presented in Table S4.

ChIP sequencing analysis

The reads were trimmed and uniquely mapped to human reference genome (hg19) using Bowtie2[2]. After duplicated reads were removed, we used model-based analysis of ChIP-seq (MACS2) peak caller[3] to identify peaks against its corresponding input with q value cutoff 0.01. Any peak in CTL −Dox group that overlapped a peak in +Dox group was removed for analyses.

For genomic classification of enriched peaks, ChIPseeker[4] was used. To discover ETV2-binding motifs, 500-bp sequences of top 3400 peaks (40% of all peaks) were applied to MEME-ChIP[5]. We identified target genes of the peaks by submitting peak regions to GREAT[6] using default settings and used for subsequent analyses. Gene ontology analysis was performed using PANTHER (http://www.pantherdb.org) or DAVID (david.abcc.ncifcrf.gov). Peaks were visualized using the Integrated Genome Browser (http://bioviz.org/igb/)

Reactive oxygen species (ROS) detection

ROS levels were measured by CellROX Deep Red reagent (C10422, Invitrogen) according to manufacturer's instructions. The cells were maintained in the EGM-2 and pre-treated with vehicle (DMSO) or forskolin for 1 hour. Subsequently, CellROX reagents were applied to cultured cells at a final concentration of 5 μM for 40 minutes at 37°C. After washing with PBS three times, the cells were harvested and resuspended in PBS. The oxidative stress levels in each group were analyzed by flow cytometry.

Co-immunoprecipitation assay

Cells were lysed with NP40 buffer. 50-μg aliquots of the lysates were incubated with 1 μg of anti-ETV2 antibody or

control IgG antibody for overnight at 4°C. Then, proteinA/G-agarose (Santa Cruz biotechnology) was added and samples were rotated for 4 hours at 4°C. Immunoprecipitates were centrifuged and the pellets were washed three times with lysis buffer. Immunocomplexes were then eluted by adding sample buffer and boiled for 3 minutes. Samples were then subjected to immunoblotting.

RNA sequencing analysis

RNA isolation was performed using TriZol Reagent (Invitrogen). For each RNA sample, the library construction was performed using the SENSE 3′ mRNA-Seq Library Prep Kit (Lexogen) according to the manufacturer's instructions. High-throughput sequencing was performed as single-end 75 sequencing using NextSeq 500 (Illumina). RNA-seq reads were aligned to the UCSC hg19 genome build. Heatmaps were generated by Cluster 3.0 and visualized using Treeview.

Gene ontology analysis was conducted on differentially expressed genes more than 2 folds between the vehicle- and forskolin-treated groups. PANTHER (http://www.pantherdb.org) was used for analyzing gene lists of up-regulated genes for overrepresented GO terms. GO-biological process was used as annotation data set (released 20171205).

For GSEA analysis, forskolin-treated group was compared to vehicle-treated group using GSEA v3.0 program. Weighted enrichment scores were calculated by ranking genes in “Diff_of Classes” metrics. The minimum and maximum gene set sizes were set to 15 and 500, respectively; the number of permutations was set to 1,000.

Quantitative RT-PCR and RT-PCR

Total RNAs were extracted from cell lysate using TriZol Reagent (Invitrogen) and reverse-transcribed using the Superscript III First-Strand Synthesis System (Invitrogen) according to the manufacturer’s instructions. With the synthesized cDNA, quantitative PCR was performed using SYBR Green PCR Master Mix (Applied Biosystems). ABI 7300 was used to quantify expression level of each gene. The amount of target RNA was normalized relative to the amount of GAPDH as a housekeeping control. Three independent analyses were conducted. The primers used in this study are shown in Table S4.

Western blots and pull-down assay

By using PRO-PREP (iNtRon biotechnology, Korea), proteins were extracted from the cells. Whole cell lysates were sonicated. Protein concentration was measured by DC assay kit (Bio-Rad, USA) according to the manufacturer's protocol. Proteins were subjected to SDS-PAGE to separate based on their molecular weight, followed by transferred to nitrocellulose membranes at 100V and 350 mA for 4 hours. The membranes were blocked with 3% Bovine Serum Albumin (BSA, GenDepot) for 60 minutes and probed with the following primary antibodies: anti-GAPDH (AB2302, Millipore), anti-ETV2 (ab181847, Abcam), anti-JUNB (sc8051, Santa Cruz Biotechnology), anti-NR4A1(sc365113, Santa Cruz Biotechnology), anti-phospho CREB (#9198, Cell Signaling Technology), anti-AKT (#4691, Cell Signaling Technology), and anti-phospho AKT (#4060, Cell Signaling Technology) in 4°C overnight. Then HRP-conjugated secondary antibodies capturing mouse or rabbit IgG (Invitrogen) were used as appropriate. Amersham Enhanced chemiluminescence (ECL) detection kit (GE Healthcare) was used to detect the secondary antibody binding and the protein bands were detected by FluorChem HD2 (Alpha Innotech., CA, USA).

Pull-down assay for detecting active Rap1 was performed using Active Rap1 Pull-down and Detection Kit (Thermo Scientific). ETV2-hDFs were cultured with or without doxycycline for 3 days and starved (0.5% FBS) overnight before stimulation with the appropriate small molecules. Cells were lysed with lysis/binding/wash buffer and incubated with glutathione agarose resin and GST-RalGDS Rap-binding domain for 1 hour at 4°C with gentle rocking. The mixture was washed 3 times with lysis/binding/wash buffer and eluted with sample buffer for immunoblotting analysis. GTP-bound Rap1 and total Rap1 was detected using anti-Rap1 antibody and EPAC1 was detected by anti-EPAC1 antibody (#4155, Cell Signaling Technology).

Annexin V apoptosis assay

Cells were harvested and resuspended in PBS at 2 x 10^5 cells per 50 μL. The cells were incubated with Flour 647-conjugated Annexin V (A23204, Invitrogen, USA) for 15 minutes in 4℃. After washing with PBS, the cells were stained with Propidium iodide (556463, BD bioscience) and subsequently analyzed by FACS Calibur (BD bioscience). Data were analyzed using FlowJo software.

FITC-dextran permeability assay

Permeability across the monolayer cultured cells was measured by using collagen type I-coated transwell plates (0.4-

μm pore size polycarbonate filter, Corning). After serum starvation in Endothelial basal medium-2 (EBM-2, Lonza) containing 1% FBS for 4 hours, the cells were treated with the inflammatory cytokines for 24 hours: TNF-α (peprotech), IL1-β (peprotech), and LPS (Sigma). Permeability was measured by adding 1 mg/ml FITC-dextran (70 kDa, Sigma) to the upper chamber. After 20 minutes of incubation, samples in the lower compartment were diluted with PBS and fluorescence was measured at excitation and emission wavelengths of 465 nm and 530 nm, respectively.

Acetylated-LDL uptake assay

To assess the ability to uptake LDL in induced endothelial cells, acetylated LDL labeled with 1,1'-dioctadecyl-3,3,3'3'-tetramethylindo-carbocyanine perchlorate (DiI-Ac-LDL, Invitrogen) was applied. The cells were incubated with 10 μg/ml DiI-Ac-LDL for 4 hours at 37°C. Fluorescence signals were photographed by confocal laser scanning microscope.

Decellularization of rat liver

All rat experiments were approved by Seoul National University Institutional Animal Care and Use Committee (SNU-151021-4-1). Rat livers were decellularized as previously described[7]. Briefly, native livers were harvested from 8-week-old male Sprague-Dawley rats (250-300 g) after systemic heparinization through cannulated hepatic vein. The scaffolds were perfused with 0.1% SDS in deionized water for 4 hours and washed with PBS for 10 hours. Median lobe of the liver scaffold was dissected, followed by sterilization of the scaffold with 0.1% peracetic acid (PAA; Sigma). The sterilized scaffolds were washed with antibiotic-containing PBS (100 U/ml Penicillin, 100 μg/ml Streptomycin) for at least 6 hours and stored at 4°C until recellularization.

Recellularization of decellularized rat liver scaffold

An overview of production of re-endothelialized livers is illustrated in Figure 4E. To delivery cells into decellularized rat livers, custom-made bioreactor perfusion system was constructed inside 37°C CO_2 incubator. All growth media were filtered before use. Before seeding the cells, the scaffolds were stabilized by perfusion of FGM-2 for an hour. 3 million of VEGFR2-sorted cells were suspended in media and injected into the scaffold at 0.5 ml/min through portal vein. Seeded scaffolds were maintained in static culture for 2 hours and then the media was perfused from the reservoir

at a rate of 1.5 ml/min by peristaltic pumps via silicone tubing. The perfusate drains passively through the outlet of the scaffold (inferior vena cava). The scaffolds were maintained in FGM-2 supplemented with 10% FBS, 1% P/S and 0.1 mg/ml Primocin (InvivoGen) for 7 days. From day 7, the medium was changed to EGM-2 containing doxycycline. At day 9, the medium was further supplemented with 5 μM forskolin. Finally, re-endothelialized livers were harvested on day 21.

To identify endothelialized areas in the scaffold, samples were fixed in 4% paraformaldehyde for 24 hours and embedded in paraffin. The paraffin blocks were sectioned serially into 5 μm thickness and stained with picrosirius red solution (0.1% Direct red 80 and 0.1% Fast green FCF, Sigma). Representative images were visualized using Nikon NIS-Elements software and a light microscope (Nikon). Also, tissue slices were stained with rhodamine-labeled Griffonia Simplicifolia Lectin I (BSL I, Vector Laboratories), anti-VE-cadherin and anti-CLDN5 respectively in accordance with the procedures stated in Immunocytochemistry. Stained signals were detected by confocal microscope.

In vivo Matrigel plug assay and hindlimb ischemia model

For Matrigel plug assay, a total of 1 x 10^6 cells was labeled with Vybrant CFDA SE Tracer kit (Invitrogen) based on manufacturer's recommendations. Labeled cells were mixed with 300 μl of Matrigel supplemented with 300 ng/ml VEGF 165 (Peprotech), 300 ng/ml bFGF (Peprotech), and 10 U/ml heparin (Sigma). Matrigel was then injected subcutaneously to the flanks of 12 week-old male athymic mice (Balb/c Nude, Nara-Biotec, Korea). Mice were supplied with 1 mg/ml doxycycline via drinking water for 14 days and was perfused with rhodamine-labeled BSL I by intravenous injection 20 minutes prior to sacrifice. Harvested Matrigel plug was fixed in 4% paraformaldehyde overnight, and saturated with 30% sucrose for 48 hours.

To induce hindlimb ischemia, 6 week-old male athymic mice (Balb/c Nude, OrientBio, Korea) were used. After anesthesia, the mice were subjected to ligation of femoral artery at proximal and distal end with single knots. Then the proximal and distal end of femoral artery were transected. A total of 5 x 10^5 cells labeled with CFDA-SE was injected collaterally from proximal to distal transected sites in each group. After transplantation of those cells, skin was sutured closed. For measurement of blood flow recovery, laser Doppler imaging analysis was conducted under anesthesia at 0, 4, 7 and 14 days after surgery. At 18 days postsurgery, the mice were perfused with rhodamine-labeled BSL1 by intravenous injection 20 minutes prior to sacrifice for tissue harvest. For histological analysis, limbs were fixated with 4% paraformaldehyde in 4°C for 48 hours and transferred to 30% sucrose solution in 4°C subsequently.

Tissues were embedded into Tissue-Tek Optimum Cutting Temperature compound (O.C.T. compound, Sakura Finetek, USA) and stored in -80°C overnight. Embedded limb tissues were consecutively sectioned at 20 μm thickness using cryostat (CM 3050, Leica, Wetzlar, Germany). The staining procedure was performed as described in Immunocytochemistry. Briefly, after washing with PBS twice, tissue sections were fixated with 4% paraformaldehyde for 10 minutes. Then, DAPI was used for nuclei staining and the sections were mounted in fluorescent mounting medium. Confocal microscope was used for visualization.

For establishment of severe hindlimb ischemia, 12 week-old male athymic mice (Balb/c Nude, Nara-Biotec, Korea) were used. Hindlimb ischemia was induced unilaterally by excision of femoral artery, vein and its branches. A total of 1 x 10^6 cells labeled with CFDA-SE was injected collateral to excised sites. Limb scoring and imaging were performed twice a week. Three weeks later, after the mice were perfused with rhodamine-labeled BSL I intravenously, gastrocnemius muscles were dissected and immediately fixed with 4% paraformaldehyde for 24 hours. Then the tissues were embedded in paraffin for histological assessment. Tissue slices were stained with hematoxylin and eosin (Sigma). After rinsed with tap water and dehydrated through an ascending series of ethanol, the sections were mounted and visualized using Nikon NIS-Elements software and a light microscope (Nikon). The immunocytochemistry staining procedure was performed as described above. All mouse experiments were approved by SNU IACUC (SNU-170202-1).

Data access

The sequence data can be accessed through the Gene Expression Omnibus (GEO) under NCBI accession number GSE123908.

Statistical analysis

At least three independent experiments were performed. All values were reported as mean ± standard deviation. A value of $p<0.05$ was considered significant. Statistical analysis between two groups was performed by unpaired, two-tailed Student's t-test. For comparison in hindlimb ischemia, two-way ANOVA was performed with Bonferroni Correction.

Supplemental References

1. Kang, I, Lee, BC, Choi, SW, Lee, JY, Kim, JJ, Kim, BE, *et al.* (2018). Donor-dependent variation of human umbilical cord blood mesenchymal stem cells in response to hypoxic preconditioning and amelioration of limb ischemia. *Exp Mol Med* **50**: 35.
2. Langmead, B, and Salzberg, SL (2012). Fast gapped-read alignment with Bowtie 2. *Nat Methods* **9**: 357-359.
3. Zhang, Y, Liu, T, Meyer, CA, Eeckhoute, J, Johnson, DS, Bernstein, BE, *et al.* (2008). Model-based analysis of ChIP-Seq (MACS). *Genome Biol* **9**: R137.
4. Yu, G, Wang, LG, and He, QY (2015). ChIPseeker: an R/Bioconductor package for ChIP peak annotation, comparison and visualization. *Bioinformatics* **31**: 2382-2383.
5. Machanick, P, and Bailey, TL (2011). MEME-ChIP: motif analysis of large DNA datasets. *Bioinformatics* **27**: 1696-1697.
6. McLean, CY, Bristor, D, Hiller, M, Clarke, SL, Schaar, BT, Lowe, CB, *et al.* (2010). GREAT improves functional interpretation of cis-regulatory regions. *Nat Biotechnol* **28**: 495-501.
7. Uygun, BE, Soto-Gutierrez, A, Yagi, H, Izamis, ML, Guzzardi, MA, Shulman, C, *et al.* (2010). Organ reengineering through development of a transplantable recellularized liver graft using decellularized liver matrix. *Nat Med* **16**: 814-820.